



PII S0016-7037(96)00109-3

A petrologic, chemical, and isotopic study of Monument Draw and comparison with other acapulcoites: Evidence for formation by incipient partial melting

T. J. McCoy,^{1,2} K. Keil,^{1,3} R. N. Clayton,⁴ T. K. Mayeda,⁴ D. D. Bogard,² D. H. Garrison,²
G. R. Huss,⁵ I. D. Hutcheon,^{5,*} and R. Wieler⁶

¹Hawaii Institute of Geophysics and Planetology, School of Ocean and Earth Science and Technology,
University of Hawaii at Manoa, Honolulu, HI 96822, USA

²NASA/Johnson Space Center, Code SN4, Houston, TX 77058, USA

³Hawaii Center for Volcanology, University of Hawaii at Manoa, Honolulu, HI 96822, USA

⁴Enrico Fermi Institute, University of Chicago, Chicago, IL 60637, USA

⁵Division of Geological and Planetary Sciences, California Institute of Technology, Pasadena, CA 91125, USA

⁶ETH Zürich, Isotopengeologie NO C61, CH-8092 Zürich, Switzerland

(Received April 18, 1995; accepted in revised form March 26, 1996)

Abstract—We have conducted petrologic, chemical, and isotopic studies of acapulcoites (Acapulco, Monument Draw, Yamato 74063, ALH A77081, ALH A81261, ALH A81315, ALH 78230, ALH A81187 and ALH 84190) in an attempt to constrain their genesis. Acapulcoites have distinctly different oxygen isotopic compositions than silicate inclusions in IAB and IIICD irons, winonaites and ureilites and, thus, formed on a different parent body. Oxygen isotopic compositions, which are slightly heterogeneous within the group, overlap with lodranites, indicating a likely origin on a common parent body. These groups can be distinguished on the basis of mafic silicate grain size. All acapulcoites have mafic silicate compositions intermediate between E and H chondrites, roughly chondritic mineralogies, achondritic, equigranular textures, micrometer to centimeter sized veins of Fe,Ni-FeS which cross-cut silicate phases, rapid metallographic cooling rates at ~600–400°C (10³–10⁵°C/Myr) and trapped noble gas abundances comparable to type 3–4 ordinary chondrites. They exhibit variable mafic silicate zoning, abundance of Fe,Ni-FeS veins, REE abundances and patterns and, possibly, cosmic ray exposure ages (~5–7 Ma). Monument Draw and Yamato 74063 retain rare relict chondrules. Phosphates are associated with Fe,Ni-FeS veins or form separate veins in Monument Draw and Acapulco. Heating and cooling of acapulcoites occurred very early in the history of the Solar System, as evidenced by the ³⁹Ar-⁴⁰Ar ages of ~4.51 Ga. These ages appear distinctly younger than the likely formation time for Acapulco of 4.557 Ga, but are older than analogous ³⁹Ar-⁴⁰Ar ages for most chondrites.

Acapulcoites formed from a precursor chondrite which differs from known chondrites in mineral and oxygen isotopic compositions. Heating to ~950–1000°C resulted in melting at the Fe,Ni-FeS cotectic, but silicates did not melt. Silicate textures resulted from extensive solid-state recrystallization. Heating was by noncollisional sources (e.g., ²⁶Al, electromagnetic induction). Despite uncertainties owing to a lack of data, acapulcoites may have experienced a three-stage thermal history of slow cooling at high temperature, rapid cooling at intermediate temperatures, and slow cooling at low temperatures, possibly resulting from breakup and gravitational reassembly of the parent body. The complex thermal history is also reflected in disequilibrium REE abundances. One or at most two impact events (~7 Ma and possibly ~5 Ma ago) are consistent with the cosmic ray exposure ages of all four acapulcoites for which cosmogenic noble gas data exist.

1. INTRODUCTION

Meteorites from asteroids come principally from two types of parent bodies, those that were heated but did not melt (primitive asteroids), and those that melted (differentiated asteroids). Rocks from the former are the chondrites, and rocks from the latter are the differentiated achondrites, stony-irons, and irons. In recent years, much effort has gone into deciphering the igneous histories of differentiated asteroids, based on studies of differentiated meteorites and a wide range of theoretical considerations (e.g., Taylor et al., 1993, and references therein). Of special significance for understanding the igneous histories of asteroids are rocks which have properties that place them between the unmelted chon-

drites and the igneous achondrites, i.e., rocks that have experienced partial, but not total melting. We suggest that two such groups of meteorites, the acapulcoites and lodranites, experienced different degrees of partial melting on a common parent body. This paper is the first in a series on the petrologic, geochemical, and isotopic properties of the acapulcoite-lodranite group and the history of its parent body and deals with the acapulcoites; lodranites and the unique meteorite LEW 86220 are discussed in separate papers (McCoy et al., 1996a,b). Here, we outline criteria for distinguishing acapulcoites from other groups of meteorites and discuss the properties of acapulcoites. We have extensively studied the newly recovered acapulcoite Monument Draw and compare it to other acapulcoites. We show that Monument Draw exhibits spectacular macroscopic and microscopic manifestations of properties present in all acapulcoites. We conclude that acapulcoites formed by noncolli-

* Present address: Lawrence Livermore National Laboratories, PO Box 808, Livermore, CA 94551, USA.

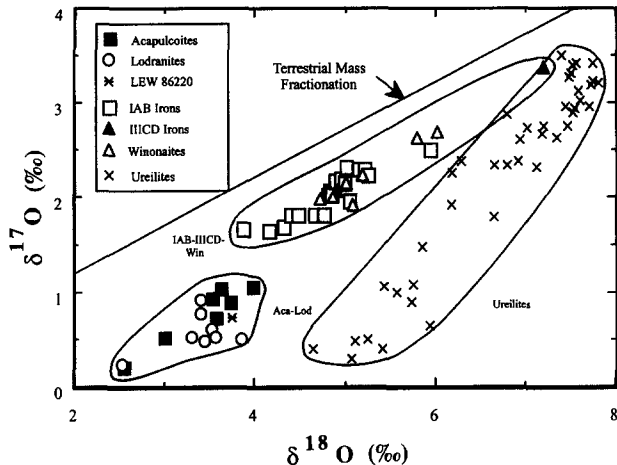


FIG. 1. Three-isotope oxygen plot for primitive achondrites, showing that acapulcoites-lodranites have essentially identical oxygen isotopic compositions, but can clearly be distinguished from other primitive achondrites as well as ureilites. Plotted are the acapulcoites Acapulco, Monument Draw, ALH A77081, ALH 78230, Yamato 74063, ALH A81187, and ALH 84190, and the lodranites Lodran, Gibson, Yamato 8002, Yamato 74357, MAC 88177, LEW 88280, EET 84302, FRO 90011; LEW 86220 is an unusual meteorite: its oxygen isotopes are typical for the acapulcoite-lodranite clan, but it consists of an acapulcoite main portion, intruded by Fe,Ni-FeS--basaltic partial melts, presumably removed from a lodranite source (from Clayton and Mayeda, 1988; Clayton et al., 1983, 1984, 1992; Franchi et al., 1992; and this work).

sional heating to temperatures of ~ 950 – 1000°C of chondritic precursor material unlike that of known chondrites. At these temperatures, cotectic melting of Fe,Ni-FeS as well as melting of phosphates took place; silicates did not melt. We further show that acapulcoites experienced a complex cooling history, possibly related to breakup and gravitational reassembly of their parent body.

2. CLASSIFICATION

Among the unusual meteorites recovered in Antarctica and elsewhere are some with mafic mineral compositions intermediate between enstatite and ordinary chondrites; they have roughly chondritic (primitive) bulk compositions, but distinctly achondritic textures. These include silicate inclusions in IAB and IIICD irons, the stony-iron lodranites, and stones similar to Acapulco and Winona. These meteorites have collectively been dubbed primitive achondrites (Prinz et al., 1983).

Acapulcoites-lodranites have characteristic oxygen isotopic compositions which set them apart from other groups of primitive achondrites. This distinction had previously been obscured by the severe terrestrial weathering and contamination that many of the Antarctic meteorites exhibit. However, this problem has largely been overcome by acid-washing of the samples prior to analysis. Improved whole-rock oxygen isotopic compositions of the acapulcoites, lodranites, and of the unusual meteorite LEW 86220 show essentially complete overlap (Fig. 1), suggesting origin on one parent body. However, they are clearly different from other primitive achondrites, suggesting that the acapulcoite-lodranite parent body was different from those of other primitive achondrites (Fig. 1). A number of other primitive achondrites which may be members of the acapulcoite-lodranite group, have not been adequately studied for oxygen isotopic compositions. Samples of Yamato 75274 and Yamato 791493 were not acid-washed when analyzed by Clayton et al. (1984). Due to the small sizes of these meteorites, no material is available to analyze acid-washed samples. Samples of ALH A81261, ALH

A81315 and Yamato 791491 were not available for oxygen isotopic analyses. However, their petrological, mineralogical and chemical properties suggest that they are members of the acapulcoite-lodranite group.

A number of chemical and physical criteria can be used to distinguish acapulcoites from lodranites. Of these, the one which can be applied most easily is the grain size of the mafic silicates (Fig. 2). Acapulcoites have smaller average grain sizes (150 – $230\ \mu\text{m}$), whereas lodranites have larger ones (540 – $700\ \mu\text{m}$). Elephant Moraine (EET) 84302 is intermediate in grain size ($340\ \mu\text{m}$), but for other reasons is classified as a lodranite. As we show in a subsequent paper (McCoy et al., 1996a), lodranites have been heated to higher temperatures and suffered greater degrees of partial melting, including silicate partial melting. We classify as acapulcoites the meteorites Acapulco, Monument Draw, Yamato 74063, ALH A77081, ALH A81315, ALH A81261, ALH 78230, ALH A81187, and ALH 84190, and as lodranites the meteorites Lodran, Gibson, Yamato 791491, Yamato 791493, Yamato 74357, Yamato 8002, Yamato 75274, MAC 88177, LEW 88280, EET 84302, and FRO 90011. Mason (1995) recently classified QUE 93148 as a lodranite based on its petrographic properties. LEW 86220 also belongs to this group, based on an oxygen isotopic composition that is typical of the acapulcoite-lodranite suite. However, it is unique in that it consists of an acapulcoite main portion, which is intruded by Fe,Ni-FeS-basaltic partial melts, presumably of lodranite parentage (McCoy et al., 1996b). Based on texture, mineralogy, mineral chemistry, and find location, it appears that the nine acapulcoites represent five distinct falls. Score and Lindstrom (1990) note that ALH A77081, ALH A81261, and ALH A81315 are paired. Petrology (Yanai and Kojima, 1987) and find locality (Yanai, 1984) strongly suggest that ALH 78230 is also paired with these meteorites. Score and Lindstrom (1990) further suggested that ALH A81187 and ALH 84190 are paired; this is consistent with our petrologic and textural data.

3. SAMPLES AND TECHNIQUES

We have conducted petrologic, chemical and isotopic studies of eight of the nine acapulcoites (all except Yamato 74063). The recovery of Monument Draw has not been previously reported in the literature. Monument Draw was found in 1985 by Joe Don Nevill as a single stone of 524.5 g near Monument Draw, Andrews County, Texas, USA ($32^\circ 30.2' \text{N}$, $102^\circ 44.6' \text{W}$), about 18 miles northwest of Andrews, Texas, USA, and is the major focus of this study. It was plowed up in a field and not recognized as a meteorite until 1990. At that time, Dr. Vestal Yeats of Texas Technical University removed a 123.9 g end piece, which was sent to Glenn Huss for

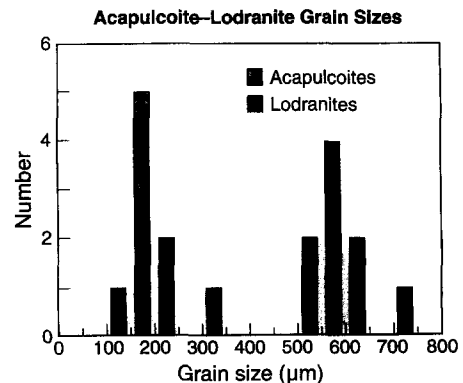


FIG. 2. Average grain sizes (μm) of individual acapulcoites and lodranites. Acapulcoites have small average grain sizes (150 – $230\ \mu\text{m}$), while most lodranites have larger average grain sizes (540 – $700\ \mu\text{m}$). Only a small number of grains could be measured from Yamato 8002, resulting in greater uncertainties in the mean grain size ($700\ \mu\text{m}$). Elephant Moraine (EET) 84302 is intermediate in grain size ($340\ \mu\text{m}$), but for other reasons is classified as a lodranite.

examination and cutting, whereas the main mass remained with the finder and is unavailable for study. The 123.9 g specimen was cut into thirds and divided between Yeats (H498.2), Huss (H498.1), and Texas Technical University. Yeats then traded his material to Walter Zeitschel of Germany. We have sampled and studied both H498.1 and H498.2. Both have weathered original surfaces. The cut faces are black, with prominent, centimeter-sized metal veins.

We studied in transmitted and reflected light polished thin sections (PTS) of Monument Draw (UH 149, 187, and 239 from H498.1; Zeitschel PTS from H498.2), Acapulco (USNM 5967; UH 165; ASU section from ASU #1163), ALH A77081 (NIPR, 51–3; MWG, 12 and, 5), ALH 78230 (NIPR, 51–3), ALH A81261 (MWG, 8), ALH A81315 (MWG, 3), ALH A81187 (MWG, 8), and ALH 84190 (MWG, 8). No section of Yamato 74063 was available for study. The maximum dimension of twenty-five mafic silicate grains in a single section was measured to determine the average grain size. Of these grains, twenty-three were randomly selected. We also sought the largest and smallest grains in each meteorite. Inclusion of these grains did not significantly affect the average grain size. Olivines poikilitically enclosed in pyroxenes were not included in these measurements, since they did not grow by the same mechanism as other grains. While averages calculated from a small number of grains carry large standard deviations, they sufficiently illustrate the gross differences in grain size between equilibrated ordinary chondrites, acapulcoites, and lodranites, and it is for this purpose that we will use this data later in the paper.

Mineral compositions were measured on a Cameca Camebax and a Cameca SX-50 electron microprobe at the University of Hawaii. Natural and synthetic compounds of well-known compositions were used as standards. Analyses of phosphates were conducted using the technique described in McCoy et al. (1994). Modal analysis of Monument Draw was conducted with the electron microprobe, using for mineral identification semiquantitative analyses with 1 second counts on scalers calibrated on grains whose precise compositions were previously determined by quantitative microprobe techniques. Five spectrometers monitoring counts for Si, Ca, Mg, Fe, and F allowed for distinction among all mineral phases. Fluorine was used for distinction between apatite and whitlockite. Metallographic cooling rates of three acapulcoites were determined using the method of Wood (1967), with the revised cooling rate curves of Willis and Goldstein (1981). Polished thin sections were etched with a mixture of 2% nitric acid in alcohol to reveal the kamacite-taenite structure, and measurements were made in the approximate centers of semi-equant taenite grains, the majority of which were rimmed by kamacite. The point within each taenite with the minimum Ni content was selected using 1 second count times on a LIF crystal calibrated on the NiK peak. These taenite grains have average phosphorus contents of <0.02 wt% and therefore should give reliable metallographic cooling rates.

Trace element abundances in phosphate and silicate phases in Monument Draw (PTS UH 239) were determined with PANURGE, a modified Cameca IMS-3f ion microprobe (Huneke et al., 1983) using energy filtering techniques similar to those described by Kennedy and Hutcheon (1992) and Kennedy et al. (1993). Absolute concentrations were calculated for Ca-normalized sensitivity factors determined from analyses of glass and mineral standards spanning the compositional range of the Monument Draw minerals. Standards included Angra dos Reis pyroxene and whitlockite, Durango apatite, fassaitic pyroxene glass, and Moore County eucrite plagioclase. Fluoride interferences in Monument Draw fluorapatite were corrected following the approach given by Zinner and Crozaz (1986).

Samples of Monument Draw (H498.2) were also analyzed for noble gases at ETH, Zürich, Switzerland, and for oxygen isotopes at the University of Chicago, Chicago, Illinois, USA. Noble gases were analyzed in a 119 mg chip in a single extraction at 1800°C, using mass spectrometric techniques described by Graf et al. (1990a). Krypton and xenon were separated from Ar by a charcoal trap at -90 to -100°C. Measurements of oxygen isotopic compositions were made using techniques described by Clayton and Mayeda (1963, 1983). Samples of Monument Draw, ALH A77081, ALH A81187, and ALH 84190 were acid-washed prior to isotopic analyses, to eliminate terrestrial weathering effects.

Samples of both Acapulco and Monument Draw were dated at

NASA/JSC using the ^{39}Ar - ^{40}Ar technique. A 52 mg sample of Acapulco and three samples of the NL-25 hornblende flux monitor (along with other samples) were irradiated in the Brookhaven National Lab (BNL) high flux beam reactor. The hornblende samples defined values for the irradiation constant, J , of 0.11349 ± 0.00019 , 0.11254 ± 0.00015 , and 0.11084 ± 0.00021 ; the individual uncertainties are derived from uncertainties in measured ratios, blank and reactor corrections and typical corrections of ~1% for atmospheric argon released from the hornblende at temperatures above 500°C. Values of J differ by amounts that are greater than individual uncertainties because of a flux gradient in the BNL reactor. Thus, we interpolated the known relative positions of Acapulco and two adjacent hornblendes and derived a J value for Acapulco of 0.11301 ± 0.00024 , where the error includes the uncertainty in relative positions. A 60 mg sample of Monument Draw was neutron irradiated in the Los Alamos Omega West reactor. Two samples of hornblende NL-25 defined J values of 0.03343 ± 0.00006 and 0.03394 ± 0.00006 ; the difference in J values again exceeds the individual uncertainties. However, because the orientation of the irradiation package was inverted half-way through the irradiation, it is not obvious that this difference represents a flux gradient. Thus, we adopted an average J value of 0.03368 ± 0.00026 for Monument Draw. Stepwise temperature extractions of Acapulco and Monument Draw were made in a high vacuum induction furnace equipped with a thermocouple, and the argon isotopes released were measured on a mass spectrometer. Hornblende monitors were preheated at 500°C, then extracted in a single 1550 °C step. Corrections were made to the argon isotopes for extraction blanks, radioactive decay, and reactor-produced interferences. Some characteristics of reactor corrections for the BNL and Los Alamos reactors and of the NL-25 hornblende monitor are presented by Bogard et al. (1995).

4. RESULTS

Here, we will not reiterate the results of previous investigations of the acapulcoites but, rather, focus on new results from our work on Monument Draw. However, we will compare the petrologic, mineralogic, and isotopic features of Monument Draw with data on other acapulcoites (Table 1).

4.1. Petrography, Mineralogy and Mineral Compositions

4.1.1. Texture

Monument Draw, like all other acapulcoites (Acapulco, Palme et al., 1981; ALH A77081, Takeda et al., 1980; Yamato 74063, Yanai and Kojima, 1991), consists of equigranular olivine, orthopyroxene, chromian diopside, plagioclase, Fe,Ni metal, troilite, whitlockite, chlorapatite, and chromite (Fig. 3). Recrystallization in all acapulcoites is evident from the abundant 120° triple junctions, as noted by Palme et al. (1981). Monument Draw has an average grain size of 150 μm ($\sigma = 66 \mu\text{m}$, $N = 25$) and a range from 50–720 μm , well within the range of other acapulcoites (Table 1). The meteorite is moderately weathered, with hydrated iron oxides of terrestrial origin occurring as veins, patches and pigments.

4.1.2. Modes

Modal analysis of Monument Draw was conducted on PTS UH 239 using electron microprobe qualitative analyses on a grid pattern of 870 points covering the entire section. Note that PTS UH 239 contains both Fe,Ni-FeS veins and a phosphate vein. Monument Draw is composed of (in vol%) olivine (23.3), orthopyroxene (38.6), chromian diopside

TABLE 1. Summary of mineralogical, petrological and isotopic data on acapulcoites.

	Olivine Fa	Low-Ca Px Fs	High-Ca Px Fs Wo	Plag. vol. %	Relict Chondrules?	Shock Stage	Two-pyroxene thermometer (°C)*	Geo- Size (µm)	Grain Size (µm)	Fe,Ni-FeS Veins µm	Phosphate Veins
Acapulco	11.9 (2)	12.6 (2)	5 41.3 (2)	8.8 (2)	No (1)	S1	1170 (2)	170	Yes	No	Yes
Monument Draw	10.1 (1)	10.6 (1)	4.4 46.0 (1)	9.8 (1)	Yes (1)	S1	980 (1)	150	Yes	Yes	Yes
Yamato 74063	10.9 (3)	10.7 (3)	4.4 44.5 (3)		Yes (3)		1040 (3)				
ALH A77081	10.7 (1)	10.5 (1)	4.4 44.6 (1)	4-12 (4,6,7)	Maybe (1)	S1	1040, 1050 (1,4)	170	Yes	No	No
ALH A81261	10.8 (1)	10.4 (1)	4.5 44.0 (1)	12.6 (1)	No (1)	S1	1060 (1)	160	Yes	No	No
ALH A81315	10.6 (1)	10.4 (1)	4.7 43.7 (1)	15.6 (1)	No (1)	S1	1070 (1)	160	Yes	No	No
ALH 78230	10.3 (5)	9.8 (5)	4.5 43.6 (5)	7 (7)	No (1)	S1	1090 (5)	170	Yes	No	No
ALH A81187	4.2 (1)	6.8 (1)	3.3 42.5 (1)	6.6 (1)	No (1)	S2	1130 (1)	230	Yes	No	No
ALH 84190	4.2 (1)	6.5 (1)		10.0 (1)	No (1)	S2		220	Yes	No	No

	δ ¹⁸ O	δ ¹⁷ O	Δ ¹⁷ O	Bulk REE	Ages (Ga)	Noble Gas Abundances	Cosmic-ray Exposure Age (Ma)*	Metallographic Cooling Rate	
Acapulco	3.73	0.90	-1.04 (8)†	LREE Enrich @ 1-2 X CI	(2,13) 4.7 ± 0.3 4.60 ± 0.03 4.503 ± 0.022	K-Ar (2) Sm-Nd (11) ³⁹ Ar- ⁴⁰ Ar (1)	Type 4 Trapped (2)	-6.5-7 (2)	-10 ⁵ C/Myr (1)
Monument Draw	3.63	1.04	-0.85 (8)	Flat @ 1 X CI	(13) 4.517 ± 0.011	³⁹ Ar- ⁴⁰ Ar (1)	Type 4 Trapped (1)	-6.5-7 (1)	-10 ⁴ C/Myr (1)
Yamato 74063	3.52	0.93	-0.91 (8)	Flat with small - Eu @ 1-2 X CI	(9) -4.5 4.556 ± 0.053	Rb-Sr Model (9) ³⁹ Ar- ⁴⁰ Ar (10)	Type 3 Trapped (12)	-6.4 (12)	
ALH A77081	3.57	0.73	-1.13 (8)	Flat @ 2 X CI	(6) 4.50 ± 0.15	K-Ar (6)	Type 4 Trapped (6)	-5.5 (6)	
ALH A81261				Flat @ 1 X CI	(13) 4.511 ± 0.007	³⁹ Ar- ⁴⁰ Ar (14)			-10 ³ C/Myr (1)
ALH A81315									
ALH 78230	3.97	1.07	-0.99 (8)	Slight LREE Depleted @ 1-2 X CI	(9) 4.531 ± 0.021	³⁹ Ar- ⁴⁰ Ar (10)			
ALH A81187	2.99	0.52	-1.03 (1)			³⁹ Ar- ⁴⁰ Ar (14)			No Taenite (1)
ALH 84190	2.54	0.20	-1.12 (1)						

* Reference indicates source of data used in calculations.

† Data reported in reference (8) were preliminary and have been revised in this work.

All data on shock stage, grain size and presence of veins from this work.

(Indicates probably paired samples

References: (1) This Work (2) Palme et al., 1981 (3) Yanai and Kojima, 1991 (4) Takeda et al., 1980 (5) Yanai and Kojima, 1987 (6) Schultz et al., 1982 (7) Hiroi and Takeda, 1991 (8) Clayton et al., 1992 (9) Torigoye et al., 1993 (10) Kaneoka et al., 1992 (11) Frunzhofer et al., 1992 (12) Takaoka and Yoshida, 1991 (13) Zipfel and Palme, 1993 (14) Münterhoff et al., 1996

(3.0), plagioclase (9.8), Fe,Ni metal (13.9), troilite (5.6), whitlockite (0.3), chlorapatite-fluorapatite (0.5), chromite (trace), and hydrated iron oxides of terrestrial origin (4.9). Results for major phases probably accurately reflect their abundances. Uncertainties based on number of counts are $\sim \pm 1$ vol% for minor phases (e.g., whitlockite, chlorapatite). In modal composition, this meteorite is remarkably similar to other acapulcoites (Acapulco, Palme et al., 1981; ALH A77081, Schultz et al., 1982; ALH 78230, Hiroi and Takeda, 1991). Three features of these modes are noteworthy. First, orthopyroxene is more abundant than olivine. This is consistent with the more reduced nature (e.g., lower Fa and Fs concentrations) of acapulcoites relative to ordinary chondrites. Second, plagioclase occurs in approximately chondritic (i.e., ~ 10 vol%; Van Schmus and Ribbe, 1968; McSween et al., 1991) abundance. This is the case for all acapulcoites (Table 1), although a wide range of abundances have been reported for different specimens of one and the same meteorite (e.g., 4–12 vol% for ALH A77081). Third, troilite is not depleted in Monument Draw and all other acapulcoites relative to ordinary chondrites, which typically have 5–6 wt% troilite. Note that large uncertainties exist in metal and troilite abundances, due in large part to sample heterogeneities and terrestrial weathering.

4.1.3. Relict chondrules

The only relict chondrule discovered in Monument Draw (PTS UH 187) is a relatively well-preserved, radiating pyroxene chondrule ~ 1.9 mm in maximum dimension (Fig. 4). In addition, Yanai and Kojima (1991) report relict barred olivine chondrules in Yamato 74063. Curiously, these relict chondrules are not of the porphyritic type, which is the most

abundant in ordinary chondrites (Gooding and Keil, 1981). Relict chondrules have also been noted in ALH A77081 by Schultz et al. (1982). They report orthopyroxene and olivine grains with metallic inclusions which, in some cases, delineate semicircular contours, hinting at the existence of former porphyritic chondrules. They also note the existence of feldspar with included chromites, reminiscent of feldspar-rich chondrules. Thus, relict chondrules are present in at least two, and possibly three, acapulcoites.

4.1.4. Silicate compositions

Mafic silicates in Monument Draw, as in all acapulcoites, are intermediate in FeO between ordinary chondrites and enstatite chondrites. Data for mafic silicates analyzed in this work are given in Table 2 and a summary of this data and literature data is given in Table 1. Monument Draw olivine averages $Fa_{10.1}$ ($\sigma = 0.2$, $N = 11$; range $Fa_{9.8-10.4}$) and low-Ca pyroxene averages $Fs_{10.6 \pm 0.4}$ and $Wo_{1.7 \pm 0.5}$ ($N = 11$; range $Fs_{10.1-11.4}$) (Table 2). A single chromian diopside has $Fs_{4.4}Wo_{46.0}$. Seven of the nine acapulcoites, including Monument Draw, have roughly similar mafic silicate compositions, ranging from $Fa_{10.3-11.9}$ and $Fs_{10.4-12.6}$, whereas the paired meteorites ALH A81187 and ALH 84190 have much lower Fa (4.2) and Fs (6.8, 6.5). Acapulco, Monument Draw, ALH A81187, and ALH 84190 have olivine with Fa lower than Fs of low-Ca pyroxene, although other members of the group have olivine with Fa only marginally higher than Fs of pyroxene.

Acapulcoites as a group show a range of zonation in their mafic silicates. Our work did not reveal any zonation in the silicates of Monument Draw. In contrast, Zipfel et al. (1995) report Ca zonation in olivine, orthopyroxene, and clinopy-

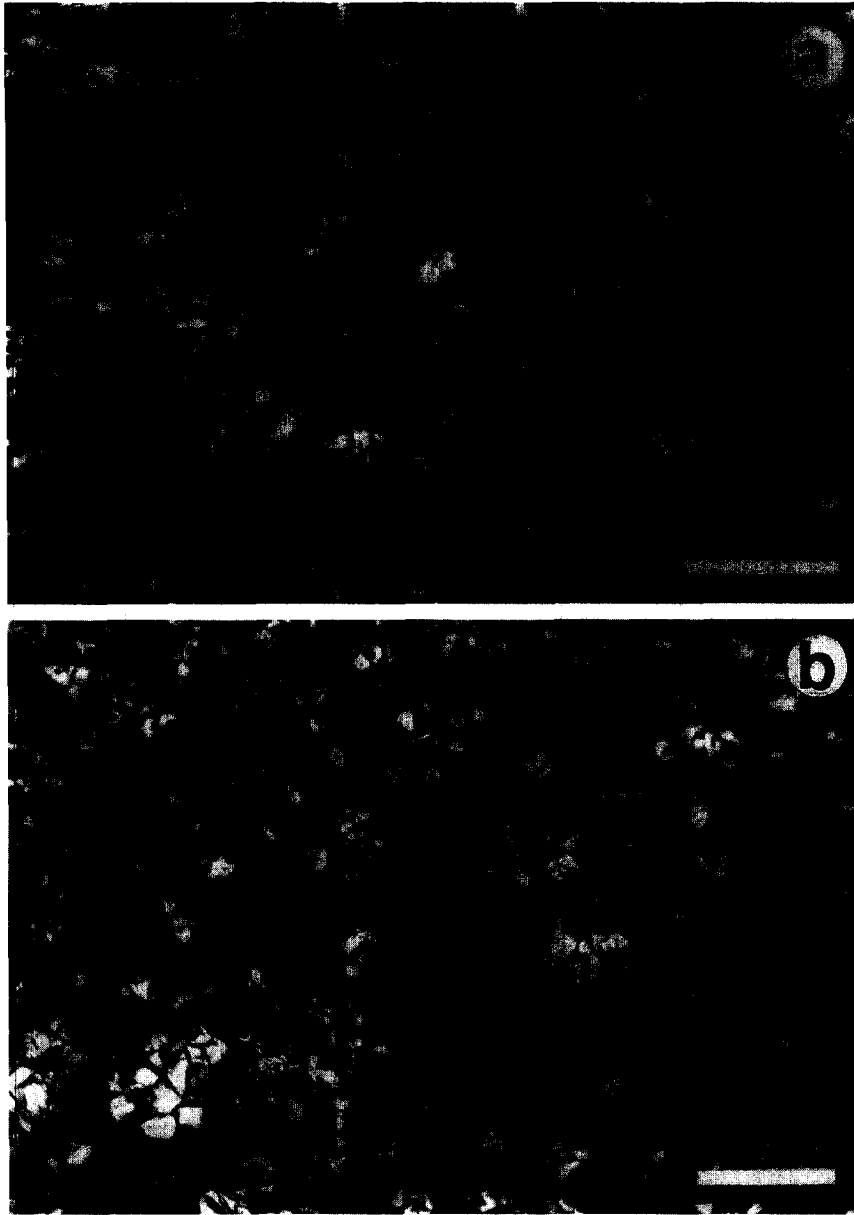


FIG. 3. Transmitted light photomicrographs in crossed polars of acapulcoite textures. Scale bars = 1 mm. (a) Monument Draw consists of equigranular orthopyroxene, olivine, chromian diopside, metal, troilite, phosphates, and minor opaques. The section is cut by numerous subparallel veinlets of terrestrial hydrated iron oxides. It appears that these veins were once filled with Fe,Ni metal and FeS. (b) Acapulco is mineralogically similar to Monument Draw. Veins of Fe,Ni-FeS, which are prominent in Monument Draw, are rare in Acapulco.

roxene in Acapulco. They found no zoning in MgO and FeO in these silicates. Takeda and Miyamoto (1994) also reported zoning within the pyroxene of Acapulco. They illustrate a depletion at the rim of orthopyroxene of CaO and Al_2O_3 and perhaps a small increase in FeO. Finally, Yugami et al. (1993) report that orthopyroxene grains in ALH A81187 show rims significantly depleted in FeO relative to their cores. Olivine grains in ALH A81187 exhibit no zoning. They attribute this feature in ALH A81187 to incomplete reduction, as supported by the relative Fa and Fs values reported above. The differences in zoning among the acapulcoites may have important implications for the thermal histories experienced by these meteorites, as discussed later.

4.1.5. Equilibration temperatures

The coexistence of low-Ca pyroxene and chromian diopside in acapulcoites allows estimation of two-pyroxene equilibration temperatures. Using the transfer equations of Kretz (1982), we calculate temperatures in the range of 980–1170°C, consistent with the highly metamorphosed textures of acapulcoites. Monument Draw yields the lowest temperature (980°C), while Acapulco yields the highest (1170°C). The paired meteorites ALH A77081, ALH A81315, ALH A81261, and ALH 78230 have equilibration temperatures ranging from 1040 to 1090°C, consistent with the relative uncertainty due to pyroxene compositional variability of



FIG. 4. Photomicrograph of the single relict chondrule, a radiating pyroxene chondrule, in Monument Draw. Transmitted, plane polarized light. Scale bar = 500 μm .

$\sim 50^\circ\text{C}$. In addition to this uncertainty, Kretz (1982) cites an uncertainty of $\pm 60^\circ\text{C}$ resulting from precision and accuracy errors. Thus, calculated temperatures may be in error by as much as 100°C . Although these temperature estimates are roughly consistent with the petrologic history of the acapulcoites, we caution against placing too much faith in the absolute values, which may be affected by errors, for example, due to the significant Cr contents of the pyroxenes. Kretz (1982) did not consider the possible influence of Cr, stating only that minor (nonquadrilateral) elements were assumed to have a negligible effect. We also note that chromian diopside is relatively rare in these meteorites and our average chromian diopside analyses were typically based on one to three analyses, often of a single grain.

4.1.6. Shock effects in silicates

We have classified Monument Draw (PTS UH 239) as shock stage S1 (unshocked) of Stöffler et al. (1991), based on study of twenty randomly selected olivines with high interference colors and sizes of 110–720 μm ; grains within 500 μm of fusion crust or poikilitically enclosed in pyroxene were excluded. All grains show sharp extinction, and only one grain required 2° of stage rotation for complete extinction. Almost all grains show irregular fractures, most of which are now filled with hydrated iron oxides of terrestrial origin. Note that Stöffler et al. (1991) also observed irregular fractures in olivines of unshocked (S1) ordinary chondrites. In addition, plagioclase does not exhibit shock effects. Some grains of other phases, notably large phosphates, have undulatory extinction. However, if these are due to shock, then the level must be much less than that which would cause undulatory extinction in olivine and, thus, classification as S1 is justified.

Palme et al. (1981) noted the unshocked nature of Aca-

pulco, and our studies indicate shock stage S1 for Acapulco, ALH A77081, ALH A81315, ALH A81261, and ALH 78230. We classified ALH A81187 and ALH 84190 as S2 (very weakly shocked), as is indicated by the undulatory extinction of olivines and a lack of planar fractures. Thus, all acapulcoites are relatively unshocked.

4.1.7. Metal-troilite

Metal and troilite occur in acapulcoites dominantly as irregular, interstitial grains of $\sim 100 \mu\text{m}$ in size, but also in lesser abundances as inclusions in mafic silicates, and as veins. Metal and troilite are commonly in contact, but do not show the tight intergrowths typical of shock-melted assemblages (Keil et al., 1992). Etching of metal grains reveals that metal in all but the low-FeO acapulcoites (ALH A81187/84190) is composed of kamacite and zoned taenite.

Ovoid inclusions and clusters of metallic Fe,Ni and, less commonly, of Fe,Ni intergrowths and isolated troilite grains, were found in orthopyroxenes and, less frequently, in olivines of Monument Draw, ALH A81315, ALH A81261, and ALH 78230, and of Acapulco (Palme et al., 1981), ALH A77081 (Schultz et al., 1982), and Yamato 74063 (Yanai and Kojima, 1991). These inclusions and clusters are ubiquitous, but are volumetrically minor ($\ll 1 \text{ vol}\%$). They tend to occur near the centers of grains, with the grain edges being free of them, with no apparent relationship to cracks in the silicates. Individual blebs vary in size, with most ranging from 5–10 μm in diameter. Allan Hills A81187 and ALH 84190 appear to contain two populations of Fe,Ni-FeS inclusions. The first population is, like those described above, dominantly Fe,Ni metal 5–10 μm in diameter and occurs in the centers of mafic silicates, with no obvious relationship to cracks. A second type found in the same

TABLE 2. Olivine and pyroxene compositions from acapulcoites analyzed in this work.

	Olivine										Orthopyroxene										Clinopyroxene									
	Monument Draw		ALH A77081	ALH A81261	ALH A81315	ALH A81187	ALH 84190	Monument Draw		ALH A77081	ALH A81261	ALH A81315	ALH A81187	ALH 84190	Monument Draw	ALH A77081	ALH A81261	ALH A81315	ALH A81187	ALH 84190	Monument Draw	ALH A77081	ALH A81261	ALH A81315	ALH A81187					
Na ₂ O	b.d.	n.d.	n.d.	n.d.	n.d.	n.d.	n.d.	b.d.	n.d.	n.d.	n.d.	n.d.	n.d.	n.d.	0.74	n.d.	n.d.	n.d.	n.d.	n.d.	0.74	n.d.	n.d.	n.d.	n.d.					
MgO	47.1	48.4	48.3	48.2	48.2	54.2	54.5	32.0	33.9	33.9	33.9	34.8	34.9	16.8	18.0	18.2	18.0	18.0	18.0	19.0	16.8	18.0	18.2	18.0	19.0					
Al ₂ O ₃	0.39	0.15	0.08	0.12	0.12	0.20	0.15	0.50	0.17	0.30	0.15	0.39	0.25	0.25	0.75	n.d.	n.d.	n.d.	n.d.	n.d.	0.75	n.d.	n.d.	n.d.	n.d.					
SiO ₂	42.1	40.0	39.9	39.8	39.8	41.5	41.7	58.3	57.3	57.3	57.0	58.0	58.2	54.5	53.8	54.1	53.8	53.8	53.8	54.4	54.5	53.8	54.1	53.8	54.4					
CaO	0.36	0.22	0.29	0.25	0.25	0.10	0.07	0.36	0.21	0.22	0.18	0.28	0.14	21.7	21.8	21.6	21.2	21.2	21.2	20.7	21.7	21.8	21.6	21.2	20.7					
TiO ₂	b.d.	b.d.	b.d.	b.d.	b.d.	b.d.	b.d.	0.24	0.19	0.20	0.20	0.05	0.18	0.53	n.d.	n.d.	n.d.	n.d.	n.d.	n.d.	0.53	n.d.	n.d.	n.d.	n.d.					
Cr ₂ O ₃	b.d.	n.d.	n.d.	n.d.	n.d.	n.d.	n.d.	0.02	n.d.	n.d.	n.d.	n.d.	n.d.	1.18	n.d.	n.d.	n.d.	n.d.	n.d.	n.d.	1.18	n.d.	n.d.	n.d.	n.d.					
MnO	0.52	0.66	0.67	0.67	0.67	0.67	0.65	0.55	0.76	0.80	0.75	0.83	0.84	0.31	0.49	0.47	0.47	0.47	0.47	0.53	0.31	0.49	0.47	0.47	0.53					
FeO	9.45	10.4	10.4	10.2	10.2	4.27	4.15	6.92	7.25	7.16	7.11	4.79	4.48	2.63	2.73	2.79	2.79	2.87	2.87	2.06	2.63	2.73	2.79	2.87	2.06					
	0.16	0.21	0.16	0.11	0.11	0.17	0.20	0.19	0.12	0.09	0.10	0.56	0.41																	
Total	99.23	99.46	99.27	98.87	98.87	100.64	101.00	99.35	100.06	99.96	99.55	100.15	100.24	99.15	96.82*	97.16*	96.34*	96.34*	96.34*	96.69*	99.15	96.82*	97.16*	96.34*	96.69*					
N	11	10	10	9	9	15	10	11	10	11	10	12	10	2	3	2	3	3	3	1	2	3	2	3	1					
Fa	10.1	10.7	10.8	10.6	10.6	4.2	4.2	10.6	10.5	10.4	10.4	6.8	6.5	4.4	4.4	4.5	4.7	4.7	4.7	3.3	4.4	4.4	4.5	4.7	3.3					
Fs	--	--	--	--	--	--	--	1.7	1.6	1.6	1.6	3.2	3.4	46.0	44.6	44.0	43.7	43.7	42.5	42.5	46.0	44.6	44.0	43.7	42.5					
Wo	--	--	--	--	--	--	--	--	--	--	--	--	--	--	--	--	--	--	--	--	--	--	--	--	--					

N= Number of analyses; b.d. = below detection; n.d. = not determined

* Low totals reflect incomplete analysis of all oxides.

Italicized figures are 1σ of compositional variability; Not given for averages of ≤ 3 analyses.

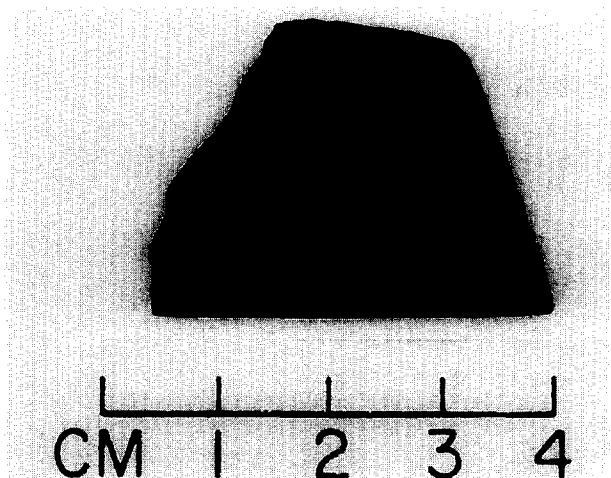


FIG. 5. Hand sample of Monument Draw exhibiting centimeter-sized veins of Fe,Ni metal.

mafic silicate grains is smaller ($1\text{--}3\ \mu\text{m}$) and occurs in parallel sets.

We discovered centimeter- to micrometer-sized veins of metallic Fe,Ni (Fig. 5) and metal plus troilite in Monument Draw, and micrometer-sized veins in all other acapulcoites we studied; veins have not previously been reported from acapulcoites. The centimeter-sized vein was seen in all hand samples of Monument Draw and appears to be entirely composed of metallic Fe,Ni, although FeS-rich network-like areas occur very near the vein. We were unable to examine the main mass of the meteorite to determine if other portions of the vein contain troilite. Microscopy indicates that the vein is composed of multiple parent taenite crystals from which numerous grains of kamacite and zoned taenite have formed. Several veins $3\text{--}10\ \text{mm}$ in length and $100\text{--}300\ \mu\text{m}$ in width are often roughly perpendicular to the centimeter-sized vein and, in a few cases, are seen to connect with the larger vein. They consist of metal and troilite, but these phases are not intimately mixed; rather, individual segments of the vein are made of either Fe,Ni metal or troilite. Finally, veins a few micrometers in width and tens to hundreds of micrometers in length are found in all acapulcoites and cross-cut all silicates including plagioclase. These veins are present at abundances $\ll 1\ \text{vol}\%$ in all acapulcoites. No precise determination of their abundance was made. In some sections of Monument Draw, numerous parallel micrometer-sized veins appear to be perpendicular to the elongation of the centimeter-sized vein. All are now dominantly filled with hydrated iron oxides of terrestrial origin, but in many places troilite occurs as segments of a few micrometers width and tens of micrometers length. Fe,Ni metal is rarer, undoubtedly because it weathers more readily than troilite. We therefore suggest that many of these micrometer-sized veins were once filled with Fe,Ni metal and troilite, which was subsequently altered by terrestrial weathering. In Acapulco, micrometer-sized veins appear to be dominated by troilite, but veins of Fe,Ni metal were also observed. In ALH A81187 and 84190, these veins are particularly well developed, are $5\text{--}10\ \mu\text{m}$ in width and hundreds of micrometers in length, and are

dominated by troilite, but a vein composed of segments of Fe,Ni metal and troilite was identified in ALH 84190. Veins are considerably less abundant and smaller ($\sim 1\ \mu\text{m}$ width, tens of micrometers in length) in the paired meteorites ALH A77081, ALH A78230, ALH A81315, and ALH A81261.

4.1.8. Metallographic cooling rates

We determined the metallographic cooling rates of three acapulcoites, all of which cooled rather rapidly through the temperature range of $600\ \text{to}\ 350^\circ\text{C}$. Etching of taenite grains reveals cores of finger plessite. In some of the acapulcoites, this finger plessite exhibits the Widmanstätten pattern. The presence of this mixture resulted in some scatter on diagrams of Ni concentrations vs. size, since individual point analyses could contain a greater amount of either kamacite or taenite. ALH A81261 exhibits such scatter and it is interesting to note that the greatest scatter exists in the acapulcoites in which the cooling rate is the slowest. Allan Hills A81261 has a reasonably well-defined cooling rate of $\sim 10^3\ \text{K/Ma}$ (Fig. 6a). Monument Draw has a somewhat faster cooling rate of $\sim 10^4\ \text{K/Ma}$ (Fig. 6b). Acapulco appears to be the most rapidly cooled acapulcoite. Taenite compositions in Acapulco are essentially invariant for grains in the radius range of $7\text{--}66\ \mu\text{m}$, and extrapolation of the cooling curves suggest a rate of $\sim 10^5\ \text{K/Ma}$ or $0.1\ \text{K/a}$ (Fig. 6c). ALH 84190 (and, presumably, the paired ALH A81187) exhibit no taenite upon etching, consistent with the low fayalite contents of its olivines relative to other acapulcoites. However, like all other acapulcoites, ALH 84190 does contain polycrystalline kamacite, consistent with rapid cooling at intermediate temperatures derived for other acapulcoites. It is interesting to note that although acapulcoites exhibit a range of metallographic cooling rates, there appears to be no correlation between cooling rate and other properties which might be indicative of the thermal history of the meteorites (e.g., two-pyroxene geothermometer temperature, grain size, $^{39}\text{Ar}\text{--}^{40}\text{Ar}$ age).

4.1.9. Phosphates

The compositions of phosphates are of particular importance to understanding the genesis of acapulcoites, not only because they are the major REE carriers, but also because preliminary work revealed evidence for phosphate mobilization and formation of phosphate veins in Monument Draw. For these reasons, we have studied in detail the phosphates in Monument Draw. Phosphates occur as interstitial grains (whitlockite, F-, and Cl-apatite), as pure phosphate veins (whitlockite), and as a constituent of large metal veins (whitlockite, less common F- and Cl-apatite). Modal analyses suggest that these phosphates account for $\sim 1\%$ of the whole rock, but errors on the mode are too large to assess the relative abundances of whitlockite and apatite. Mass balance of La using our measured mineral compositions and the bulk composition of Zipfel and Palme (1993) suggests that whitlockite is more abundant than apatite. In Acapulco, phosphates occur in similar settings, but apatite is much more abundant than whitlockite (Zipfel et al., 1995). We have discovered a $1.8\ \text{mm}$ long and $\sim 200\ \mu\text{m}$ wide vein in

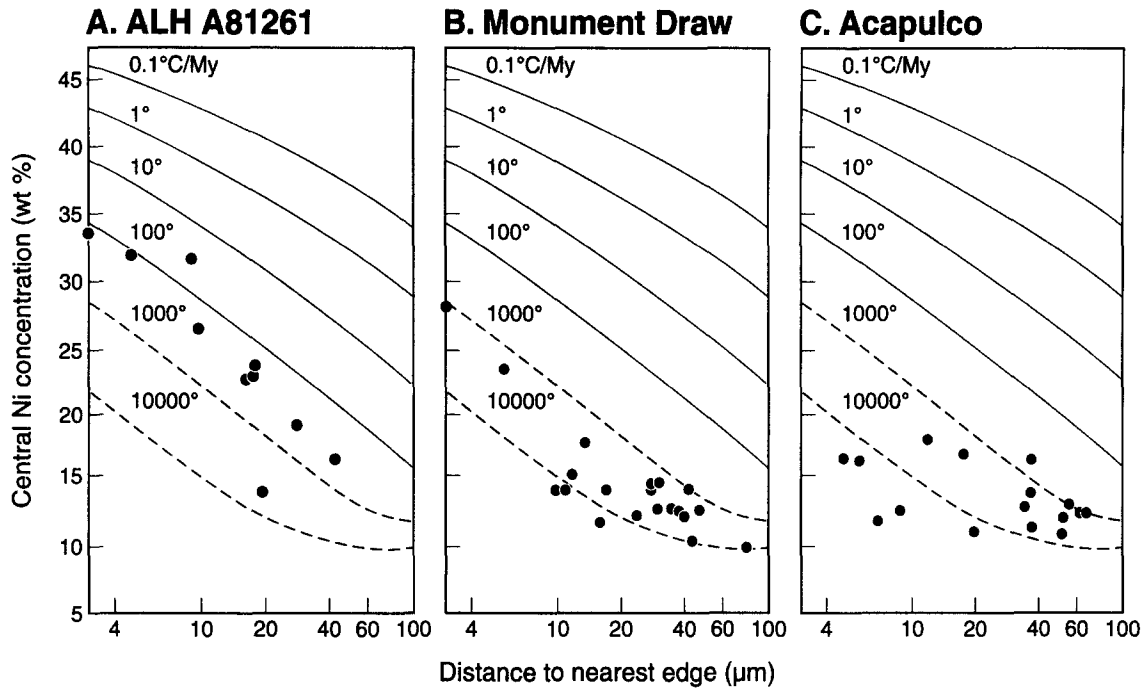


FIG. 6. Plots of central Ni content vs. distance to the nearest edge for taenite grains in acapulcoites. Curves for cooling at 0.1–100 K/Ma from Willis and Goldstein (1981). Curves for 10^3 – 10^5 K/Ma are approximate. All acapulcoites experienced rapid cooling in the temperature interval from approximately 600 to 350°C. ALH A81261 (a) cooled at $\sim 10^3$ K/Ma; Monument Draw (b) at $\sim 10^4$ K/Ma; and Acapulco (c) at $\sim 10^5$ K/Ma.

Acapulco that consists of F-Cl-bearing apatite (PTS USNM 5967).

Vein-forming phosphates. The most prominent occurrence of phosphates in Monument Draw is as whitlockite veins. One such vein in PTS UH 149 is ~ 2.5 mm long and 100–200 μm wide (Fig. 7). A linear feature in its center is now

filled with hydrated iron oxides of terrestrial origin, but may have once been Fe,Ni metal and/or troilite. In PTS UH 239, a vein of nearly identical dimensions occurs, although the section was prepared from a different piece of the meteorite. This vein (whitlockite #3) is essentially homogeneous in major and minor elements (Tables 3 and 4), with the excep-

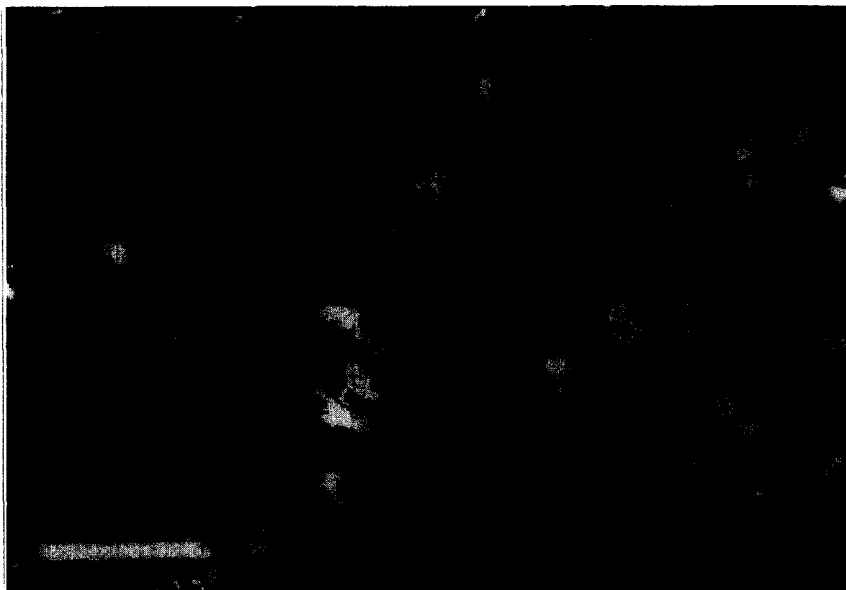


FIG. 7. Transmitted, plane polarized light photomicrograph of a whitlockite vein in Monument Draw (PTS UH 149). Scale bar = 500 μm . The prominent black line in the center of the vein is now filled with hydrated iron oxides of terrestrial origin, although we speculate that it was once Fe,Ni metal and/or troilite.

TABLE 3. Major (wt.%) element compositions of phosphates in Monument Draw.

Grain	1	1	1	1	1	2	3	3	3	3	3
Microprobe	1	2	3	4	5	6	7	8	9	10	11
Position	Rim	Core	Rim	Rim	Rim						
Mineral ¹	Cl-A	Cl-A	Cl-A	F-A	Cl-A	Whit	Whit	Whit	Whit	Whit	Whit
FeO	b.d.	0.08	0.08	b.d.	0.11	0.19	0.16	0.21	0.29	0.24	0.31
MnO	0.05	0.06	0.06	0.07	0.06	0.04	b.d.	0.04	b.d.	b.d.	b.d.
MgO	0.06	0.05	0.04	0.07	0.10	3.57	3.64	3.65	3.68	3.66	3.75
CaO	54.3	54.7	54.9	54.6	54.8	47.7	47.8	47.7	47.9	47.6	47.8
Na ₂ O	0.40	0.35	0.34	0.33	0.36	2.82	2.82	2.80	2.83	2.94	2.85
K ₂ O	b.d.	b.d.	0.03	b.d.	0.02	0.03	0.08	0.06	0.03	0.05	0.06
P ₂ O ₅	41.4	41.6	41.6	41.2	41.5	46.5	46.7	46.8	46.9	46.9	46.4
F	1.50	1.70	1.65	1.97	1.75	b.d.	b.d.	b.d.	b.d.	b.d.	b.d.
Cl	4.07	3.55	3.59	3.08	3.44	b.d.	b.d.	b.d.	b.d.	b.d.	b.d.
Total	101.85	102.11	102.46	101.37	102.13	100.84	101.09	101.30	101.58	101.29	101.15
O=Cl,F	1.55	1.52	1.51	1.52	1.51	0.00	0.00	0.00	0.00	0.00	0.00
Total	100.30	100.59	100.95	99.85	100.62	100.84	101.09	101.30	101.58	101.29	101.15
F/(F+Cl)	0.37	0.43	0.42	0.51	0.45	--	--	--	--	--	--

Grain	4	5	6	7	8	9	10	11	11	11	11
Microprobe	12	13	14	15	16	17	18	19	20	21	22
Position				F-A	F-A	F-A	Cl-A	Core	Rim	Rim	Core
Mineral	Whit	Whit	Whit	F-A	F-A	F-A	Cl-A	F-A	F-A	F-A	F-A
FeO	0.10	0.25	0.13	0.31	0.44	0.31	0.44	b.d.	0.04	b.d.	b.d.
MnO	0.06	b.d.	0.04	0.06	b.d.	0.07	0.09	0.05	0.03	b.d.	0.04
MgO	3.62	3.62	3.57	0.05	0.04	b.d.	b.d.	0.19	0.21	0.18	0.19
CaO	48.0	47.8	47.6	56.0	56.1	55.9	54.5	55.9	55.9	55.9	55.8
Na ₂ O	2.81	2.90	2.82	b.d.	b.d.	0.12	0.37	b.d.	b.d.	b.d.	b.d.
K ₂ O	0.06	0.05	0.04	b.d.	b.d.	b.d.	0.02	b.d.	b.d.	b.d.	b.d.
P ₂ O ₅	46.8	46.5	46.6	42.5	41.6	41.8	42.3	41.7	42.4	42.0	42.3
F	b.d.	b.d.	b.d.	3.70	3.58	2.65	1.18	4.31	4.03	4.21	4.08
Cl	b.d.	b.d.	b.d.	0.37	0.61	2.02	4.46	0.15	0.16	0.18	0.16
Total	101.43	101.13	100.86	103.05	102.33	102.97	103.33	102.34	102.83	102.65	102.59
O=Cl,F	0.00	0.00	0.00	1.64	1.65	1.57	1.50	1.85	1.73	1.81	1.75
Total	101.43	101.13	100.86	101.41	100.68	101.40	101.83	100.49	101.10	100.84	100.84
F/(F+Cl)	--	--	--	0.94	0.90	0.68	0.30	0.98	0.98	0.97	0.98

¹ Whit = Whitlockite; Cl-A = Chlorapatite; F-A = Fluorapatite; Cl- vs. F-apatite based on F/(F+Cl)
b.d. = below detection limits

tion of Fe, which has been extensively mobilized in Monument Draw by terrestrial weathering. The REEs in whitlockite #3 are enriched to 100–200 × CI and the HREE abundances vary by about a factor of two within the vein (Table 4, Fig. 8a). LREEs are slightly enriched relative to HREEs (CI-normalized La/Yb ≈ 1.5) and there is a prominent negative Eu anomaly (Fig. 8a).

Phosphates are also a prominent component of the millimeter- to centimeter-sized Fe,Ni-FeS veins in Monument Draw. Multiple major and/or minor element analyses were conducted on two whitlockite grains (#2, 5) associated with the largest vein. Whitlockite #2 is a millimeter-sized, irregular grain with REE abundances of ~150 × CI and a less fractionated REE pattern than that in vein #3. Abundance variations from point to point are barely outside of measurement uncertainty (Fig. 8b; Table 3). Whitlockite #5 is also a millimeter-sized irregular grain with homogeneous major, minor, and trace element contents and REE abundances similar to whitlockite #2 (Tables 3 and 4).

We also analyzed a single, semi-equant chlorapatite grain (#1) ~1mm in diameter associated with the large Fe,Ni-FeS vein. This grain has variable F and Cl contents (Table 3), but these elements do not exhibit a regular zoning pattern.

The REE pattern is nearly flat with a negative Eu anomaly and the abundances are a factor of ~3 lower than in whitlockite. At equilibrium, apatite should have roughly 5 times less REEs (Murrell et al., 1984; Davis et al., 1993). REE abundances are 30 to 50% higher and the Eu anomaly correspondingly deeper in the core of the grain compared to two spots near the edge (Fig. 8c), suggesting that the grain is zoned for REEs. Fluorapatite #11 is an ovoid (300 × 225 μm) grain associated with the large Fe,Ni-FeS vein, with four analyses at both the core and rim yielding F/(F + Cl) ratios of ~0.98 (Table 3). REE abundances in fluorapatite #11 are a factor of two higher than in apatite #1 and the abundance pattern is similar (Fig. 8c). The magnitude and sign of the difference in REE abundance between a chlorapatite and fluorapatite in such close proximity are surprising in view of the indications from liquid-crystal systems that REE concentrations in apatite should correlate positively with the Cl/(Cl + F) ratio (Murrell et al., 1984; Jolliff et al., 1993).

Interstitial phosphates. Phosphates #4,6,7,8,9,10, and 12–16 are irregularly shaped interstitial grains ranging in size from 60 μm to ~1mm. They include whitlockite, chlorapatite, and fluorapatite, with F/(F + Cl) ratios for apatite

ranging from 0.30 to 0.90 (Table 3). Grain numbers correspond to those given in Tables 3 and 4. Grains 12–16 were not analyzed for major elements by electron microprobe. One grain (#6) consists of an intergrowth of chlorapatite and whitlockite (Fig. 9). The REE patterns are similar to those of vein-forming phosphates, with whitlockites exhibiting flat patterns with a negative Eu anomaly and apatites exhibiting patterns slightly enriched in LREEs (Fig. 10). REE abundances tend to be lower in the interstitial phosphates and there is a considerable range in absolute abundance, particularly among the apatites; La concentrations vary by a factor of ~ 2 . These lower abundances do not result from beam overlap with silicates. SEM images show the SIMS analysis points to be entirely within phosphate and the Si^+ intensities are typically very low (e.g., Table 4). The large spread in abundances indicates that the REEs are not well equilibrated between Monument Draw phosphates.

Striking evidence for chemical disequilibrium can be seen in the REEs from chlorapatite #10 (Fig. 10b). This grain has relatively low REE abundances, a LREE-enriched pattern, and a positive Eu anomaly. Two analyses of apatite #10 agree well and neither SIMS crater overlaps silicates, as shown by SEM images and very low Si^+ intensity (converted to ppm Si for the second measurement, Table 4). Since phosphates typically try to exclude Eu, a positive Eu anomaly implies that the local region has a precursor highly enriched in Eu and did not produce enough plagioclase for complete uptake. The REEs were clearly not diffusing over millimeters or the excess Eu would have redistributed.

To elucidate the unusual pattern in chlorapatite #10 and to investigate further the degree of disequilibrium in Monument Draw, we measured REE abundances in plagioclase, orthopyroxene, and olivine adjacent to several of the phosphates. Plagioclase, orthopyroxene, and olivine adjacent to chlorapatite #10 exhibit low REE abundances and, except for the positive Eu anomaly in plagioclase, surprisingly similar REE patterns (Fig. 11a). There is little evidence of a local excess of Eu^{2+} . The REE patterns in all three silicates are much flatter than expected for equilibrium partitioning and the difference in REE concentrations both between apatite and the silicates and among the silicates is much less than anticipated (Richardson and McSween, 1989; Davis et al., 1993). Orthopyroxene has a CI-normalized La/Lu ratio $\sim 40\times$ higher than the equilibrium value, while the value in plagioclase is $\sim 20\times$ lower than expected. Similar behavior of the REEs is found in the mineral assemblages surrounding whitlockites #2 and #14 (Fig. 11b,c). Both whitlockites exhibit flat REE patterns with abundances of $\sim 120\times$ chondritic and negative Eu anomalies. Orthopyroxene is again characterized by a rather flat REE pattern with a much greater than expected $(\text{La}/\text{Lu})_{\text{cn}}$. Although the REE abundances and patterns in the silicates and phosphates are qualitatively consistent with equilibrium partitioning, the relative concentrations of La in whitlockite and orthopyroxene differ by only a factor of ~ 1500 – 5000 instead of the equilibrium value near $\sim 50,000$ (e.g., Davis et al., 1993). This indicates that redistribution of REEs among minerals has taken place but that equilibrium has not been achieved. The absence of equilibrium is also shown by the spread of 2 – $3\times$ in REE abundances in orthopyroxene surrounding whitlockites #2

and #14 and up to $8\times$ between orthopyroxene adjacent to whitlockite #15 (Table 4).

4.2. ^{39}Ar - ^{40}Ar Chronology

Argon isotopic data, along with the calculated ages and K/Ca ratios for each temperature extraction of Acapulco and Monument Draw, are given in Table 5. Ages have been calculated using the ^{40}K abundance and decay parameters recommended by Steiger and Jaeger (1977). Errors reported for individual ages were compounded from uncertainties in blank and reactor corrections plus analytical uncertainties in measuring the $^{40}\text{Ar}/^{39}\text{Ar}$ ratios in the samples. To facilitate comparisons of ages at different release temperatures, age uncertainties do not include uncertainties in neutron fluence (J) discussed earlier.

4.2.1. ^{39}Ar - ^{40}Ar ages

Calculated ^{39}Ar - ^{40}Ar ages and K/Ca ratios as a function of fractional release of ^{39}Ar for Acapulco and Monument Draw are shown in Fig. 12. Each meteorite defines a “plateau” of essentially constant age across a significant fraction of its ^{39}Ar release. Each meteorite also exhibits a decrease in K/Ca of more than an order of magnitude during the stepwise extractions. Monument Draw shows two distinct peaks in the rate of Ar release as a function of temperature, with minimum Ar release occurring at the temperatures of rapid change in K/Ca ratios ($\sim 70\%$ ^{39}Ar release). We have commonly observed this behavior in chondrites and achondrites and attribute it to differences in ease of Ar degassing from mineral phases having different K/Ca ratios. For Acapulco the rates of Ar release from these phases show greater overlap. The somewhat lower relative ages for the first few extractions of Acapulco (0–22% ^{39}Ar release) are attributed to recent Ar diffusive loss from low retention sites with high K/Ca, and these data are not considered in deriving the ^{39}Ar - ^{40}Ar age. Monument Draw (a find) also shows a very slightly lower age for a single extraction (1050°C at $\sim 75\%$ ^{39}Ar release) that represents early Ar release from the phase with lower K/Ca. We have previously observed this effect in weathered meteorites and attribute it to modest ^{40}Ar loss from grain surfaces of the low-K/Ca mineral phase. It is an analogous but smaller effect to that demonstrated by the first extractions of the high K/Ca phase. The very slightly elevated ages for Monument Draw at ~ 2 – 15% ^{39}Ar release are probably not due to occluded atmospheric ^{40}Ar , as we see no direct evidence for this in the isotopic data. Measured K from Ar concentrations of irradiated samples of Acapulco (535 ppm) and Monument Draw (354 ppm) are less than those of typical chondrites (Jarosewich, 1990).

Six extractions of Acapulco, releasing 22–97% of the total ^{39}Ar , define a plateau age of 4.510 ± 0.011 Ga. (The age for each extraction is weighed by the relative amount of ^{39}Ar it released, and the error is 1σ of deviations from the mean age.). Twelve extractions of Monument Draw (0.5–99% of the ^{39}Ar release) define a plateau age of 4.517 ± 0.011 Ga. If we exclude the 1050°C extraction with a slightly lower age and the 500–725°C extractions with slightly elevated ages, 81% of the ^{39}Ar released from Monu-

TABLE 4. REE and other trace-element abundances for phosphates and adjacent phases in Monument Draw (ppm wt. unless noted).

Grain	Chlorapatite			Whitlockite			Whitlockite			Whitlockite			Whitlockite		
	#1 Pt 1 Rlm	#1 Pt 2 Core	#1 Pt 3 Rlm	#2 Pt 1	#2 Pt 2	#2 Pt 3	#2 Pt 4	#2 Pt 5	#2 Pt 6	#3 Pt 1	#3 Pt 2	#3 Pt 3	#4 Pt 1	#4 Pt 2	#4 Pt 3
EMP Point	3	2	1	6	7	11	10	11	11	16	17	10	11	11	10
La	12.3 ± 1.3	14.0 ± 1.5	11.3 ± 1.2	35.8 ± 3.7	39.2 ± 4.0	38.0 ± 4.2	37.9 ± 4.2	32.8 ± 3.6	34.9 ± 3.5	41.9 ± 4.2	43.4 ± 4.4	45.0 ± 4.5	41.9 ± 4.2	43.4 ± 4.4	45.0 ± 4.5
Ce	23.4 ± 2.3	29.8 ± 3.0	22.4 ± 2.2	83.8 ± 8.5	93.4 ± 9.4	86.4 ± 8.6	85.2 ± 8.5	75.1 ± 7.5	86.7 ± 8.8	97.8 ± 9.8	104 ± 10	108 ± 11	97.8 ± 9.8	104 ± 10	108 ± 11
Pr	3.08 ± 0.34	4.18 ± 0.46	2.88 ± 0.32	11.9 ± 1.3	13.1 ± 1.3	11.9 ± 1.3	12.1 ± 1.3	10.8 ± 1.2	12.9 ± 1.3	13.3 ± 1.4	14.6 ± 1.5	14.9 ± 1.5	13.3 ± 1.4	14.6 ± 1.5	14.9 ± 1.5
Nd	15.7 ± 1.6	22.0 ± 2.2	15.0 ± 1.5	60.8 ± 6.3	67.7 ± 7.0	60.7 ± 6.1	59.2 ± 5.9	54.6 ± 5.5	61.7 ± 6.2	63.0 ± 6.4	72.1 ± 7.3	76.5 ± 7.9	63.0 ± 6.4	72.1 ± 7.3	76.5 ± 7.9
Sm	5.12 ± 0.56	6.81 ± 0.75	5.00 ± 0.55	19.0 ± 2.0	21.7 ± 2.3	19.5 ± 2.1	18.6 ± 2.0	18.7 ± 2.1	17.7 ± 1.8	17.6 ± 1.9	21.5 ± 2.3	22.8 ± 2.4	17.6 ± 1.9	21.5 ± 2.3	22.8 ± 2.4
Eu	1.03 ± 0.12	0.98 ± 0.12	1.14 ± 0.14	2.00 ± 0.24	2.08 ± 0.23	1.93 ± 0.23	1.88 ± 0.22	1.86 ± 0.22	1.60 ± 0.17	2.13 ± 0.23	2.24 ± 0.25	2.21 ± 0.25	2.13 ± 0.23	2.24 ± 0.25	2.21 ± 0.25
Gd	6.6 ± 1.3	10.0 ± 2.1	6.7 ± 1.3	20.1 ± 3.8	28.6 ± 4.1	23.0 ± 3.2	24.0 ± 3.4	14.4 ± 2.0	20.7 ± 2.2	14.5 ± 2.8	20.2 ± 4.1	23.3 ± 3.8	14.5 ± 2.8	20.2 ± 4.1	23.3 ± 3.8
Tb	1.03 ± 0.21	1.43 ± 0.28	1.07 ± 0.22	3.16 ± 0.59	4.06 ± 0.59	3.56 ± 0.53	3.61 ± 0.54	2.81 ± 0.42	4.08 ± 0.44	2.51 ± 0.45	3.34 ± 0.58	4.00 ± 0.71	2.51 ± 0.45	3.34 ± 0.58	4.00 ± 0.71
Dy	6.58 ± 0.79	9.5 ± 1.1	7.02 ± 0.84	26.3 ± 2.8	31.6 ± 3.3	27.7 ± 3.3	26.9 ± 3.2	22.2 ± 2.7	27.0 ± 2.7	21.3 ± 2.3	28.7 ± 3.1	30.1 ± 3.1	21.3 ± 2.3	28.7 ± 3.1	30.1 ± 3.1
Ho	1.44 ± 0.16	1.96 ± 0.21	1.59 ± 0.17	5.78 ± 0.61	7.16 ± 0.75	5.65 ± 0.62	5.57 ± 0.61	4.70 ± 0.52	5.43 ± 0.56	4.41 ± 0.46	6.24 ± 0.65	6.43 ± 0.66	4.41 ± 0.46	6.24 ± 0.65	6.43 ± 0.66
Er	4.60 ± 0.51	5.56 ± 0.61	4.31 ± 0.47	17.4 ± 1.8	21.2 ± 2.2	19.4 ± 2.1	18.5 ± 2.0	15.6 ± 1.7	17.5 ± 1.8	13.7 ± 1.4	19.3 ± 2.0	19.5 ± 2.0	13.7 ± 1.4	19.3 ± 2.0	19.5 ± 2.0
Tm	0.85 ± 0.07	0.80 ± 0.09	0.68 ± 0.07	2.81 ± 0.30	3.44 ± 0.38	3.02 ± 0.33	2.90 ± 0.32	2.41 ± 0.27	2.52 ± 0.26	2.39 ± 0.25	3.16 ± 0.34	3.33 ± 0.35	2.39 ± 0.25	3.16 ± 0.34	3.33 ± 0.35
Yb	4.01 ± 0.44	5.17 ± 0.57	3.94 ± 0.43	20.7 ± 2.2	21.8 ± 2.3	20.6 ± 2.3	20.2 ± 2.2	19.6 ± 2.2	19.1 ± 1.9	18.8 ± 1.9	23.1 ± 2.4	23.0 ± 2.4	18.8 ± 1.9	23.1 ± 2.4	23.0 ± 2.4
Lu	0.89 ± 0.08	0.99 ± 0.12	0.84 ± 0.10	3.64 ± 0.40	3.97 ± 0.47	2.98 ± 0.32	3.07 ± 0.37	2.75 ± 0.33	3.06 ± 0.33	3.01 ± 0.34	3.74 ± 0.41	3.39 ± 0.39	3.01 ± 0.34	3.74 ± 0.41	3.39 ± 0.39
F				< 3.2	< 4.1				4.9 ± 1.0	< 1.7	2.1 ± 1.5				
Si									59 ± 30						
Ti	738 ± 368	812 ± 405	820 ± 410	907 ± 450	1010 ± 505	835 ± 420	850 ± 425	870 ± 456	1435 ± 720	1000 ± 500	990 ± 500	1070 ± 530	1000 ± 500	990 ± 500	1070 ± 530
V	0.5 ± 0.3	0.6 ± 0.4	0.5 ± 0.3	3.3 ± 1.6	4.2 ± 2.1	2.5 ± 1.3	2.6 ± 1.3	2.0 ± 1.0	1.8 ± 0.9	4.2 ± 2.1	3.9 ± 2.0	3.7 ± 1.9	4.2 ± 2.1	3.9 ± 2.0	3.7 ± 1.9
Cr	2.3 ± 1.2	3.2 ± 1.8	3.0 ± 1.5	10.6 ± 5.3	15.9 ± 7.9	10.0 ± 5.0	9.8 ± 4.9	6.6 ± 3.3	7.5 ± 3.8	16.5 ± 8.3	16.7 ± 8.4	15.3 ± 7.7	16.5 ± 8.3	16.7 ± 8.4	15.3 ± 7.7
Sc	0.44 ± 0.22	0.40 ± 0.20	0.36 ± 0.18	6.8 ± 3.4	7.5 ± 3.8	5.9 ± 3.0	5.4 ± 2.7	4.2 ± 2.1	7.3 ± 3.7	7.3 ± 3.7	7.3 ± 3.7	7.2 ± 3.6	7.3 ± 3.7	7.3 ± 3.7	7.2 ± 3.6
Rb									12 ± 6						
Sr				34.8 ± 8.7	41 ± 10				41 ± 10	44 ± 11	43 ± 11	45 ± 11	44 ± 11	43 ± 11	45 ± 11
Ba	2.0 ± 0.4	1.7 ± 0.4	2.0 ± 0.4	0.21 ± 0.05	0.28 ± 0.06	0.19 ± 0.04	0.30 ± 0.06	0.10 ± 0.03	0.19 ± 0.04	0.66 ± 0.09	0.67 ± 0.09	0.29 ± 0.05	0.66 ± 0.09	0.67 ± 0.09	0.29 ± 0.05
Th				2.45 ± 0.30	4.08 ± 0.49				3.4 ± 0.4	2.35 ± 0.28	3.47 ± 0.42	3.03 ± 0.36	2.35 ± 0.28	3.47 ± 0.42	3.03 ± 0.36
U				0.43 ± 0.08	0.72 ± 0.13				0.60 ± 0.11	0.63 ± 0.13	0.45 ± 0.09	0.57 ± 0.11	0.63 ± 0.13	0.45 ± 0.09	0.57 ± 0.11
Grain															
EMP Point					13										
La	29.5 ± 3.0	24.4 ± 2.5	34.0 ± 3.5	36.3 ± 3.6	34.8 ± 3.5	37.5 ± 3.8	19.0 ± 2.0	18.3 ± 1.9	13.3 ± 1.4	9.12 ± 0.97	11.2 ± 1.2		9.12 ± 0.97	11.2 ± 1.2	
Ce	68.5 ± 7.0	60.9 ± 6.2	79.4 ± 8.0	84.2 ± 8.5	82.8 ± 8.4	88.0 ± 8.8	44.5 ± 4.6	42.7 ± 4.4	27.7 ± 2.8	18.9 ± 2.0	21.6 ± 2.3		18.9 ± 2.0	21.6 ± 2.3	
Pr	10.0 ± 1.3	8.4 ± 0.9	11.5 ± 1.2	12.0 ± 1.2	11.9 ± 1.2	12.6 ± 1.3	6.00 ± 0.63	5.35 ± 0.57	3.61 ± 0.38	2.47 ± 0.27	3.05 ± 0.32		2.47 ± 0.27	3.05 ± 0.32	
Nd	44.1 ± 4.4	35.4 ± 3.6	57.9 ± 5.9	63.2 ± 6.4	62.8 ± 6.4	67.4 ± 7.0	25.4 ± 2.6	24.3 ± 2.5	17.7 ± 1.9	9.32 ± 0.96	13.6 ± 1.4		9.32 ± 0.96	13.6 ± 1.4	
Sm	12.7 ± 1.3	9.5 ± 1.0	18.2 ± 1.9	19.3 ± 2.0	19.7 ± 2.1	21.1 ± 2.3	7.07 ± 0.74	6.41 ± 0.68	4.91 ± 0.55	2.12 ± 0.27	3.07 ± 0.36		2.12 ± 0.27	3.07 ± 0.36	
Eu	1.65 ± 0.17	1.53 ± 0.16	1.92 ± 0.21	1.97 ± 0.23	1.85 ± 0.22	1.97 ± 0.22	1.49 ± 0.15	1.57 ± 0.16	0.75 ± 0.11	0.62 ± 0.07	0.58 ± 0.06		0.62 ± 0.07	0.58 ± 0.06	
Gd	14.1 ± 1.5	9.5 ± 1.1	19.9 ± 3.4	22.0 ± 3.0	25.3 ± 3.7	21.2 ± 3.8	5.86 ± 0.71	7.70 ± 0.87	4.45 ± 1.4	3.01 ± 0.38	4.62 ± 0.54		3.01 ± 0.38	4.62 ± 0.54	
Tb	3.10 ± 0.33	2.00 ± 0.22	3.17 ± 0.54	3.38 ± 0.47	4.01 ± 0.57	3.47 ± 0.57	1.24 ± 0.14	1.45 ± 0.16	0.63 ± 0.16	0.47 ± 0.08	0.86 ± 0.12		0.47 ± 0.08	0.86 ± 0.12	
Dy	20.2 ± 2.0	13.0 ± 1.3	26.4 ± 2.7	28.3 ± 2.9	28.2 ± 2.9	31.1 ± 3.2	9.16 ± 0.94	9.03 ± 0.92	6.14 ± 0.70	3.34 ± 0.36	4.85 ± 0.51		3.34 ± 0.36	4.85 ± 0.51	
Ho	4.52 ± 0.47	3.00 ± 0.31	5.76 ± 0.63	6.32 ± 0.66	6.39 ± 0.66	6.94 ± 0.73	1.86 ± 0.20	1.81 ± 0.19	1.19 ± 0.16	0.73 ± 0.09	0.96 ± 0.11		0.73 ± 0.09	0.96 ± 0.11	
Er	15.3 ± 1.5	9.6 ± 1.0	17.6 ± 1.8	18.7 ± 1.9	18.7 ± 1.9	20.6 ± 2.1	6.45 ± 0.66	6.23 ± 0.64	3.62 ± 0.45	2.20 ± 0.24	2.78 ± 0.29		2.20 ± 0.24	2.78 ± 0.29	
Tm	2.33 ± 0.24	1.61 ± 0.17	2.86 ± 0.30	3.18 ± 0.33	3.07 ± 0.34	3.30 ± 0.34	1.01 ± 0.11	0.99 ± 0.11	0.64 ± 0.09	0.37 ± 0.05	0.45 ± 0.05		0.37 ± 0.05	0.45 ± 0.05	
Yb	20.0 ± 2.0	14.9 ± 1.5	20.8 ± 2.1	21.9 ± 2.3	20.2 ± 2.1	23.8 ± 2.5	9.45 ± 0.96	8.92 ± 0.91	4.26 ± 0.49	3.13 ± 0.34	3.69 ± 0.39		3.13 ± 0.34	3.69 ± 0.39	
Lu	3.28 ± 0.34	2.41 ± 0.26	3.46 ± 0.38	3.59 ± 0.38	3.36 ± 0.37	4.14 ± 0.46	1.50 ± 0.17	1.48 ± 0.17	1.03 ± 0.20	0.70 ± 0.09	0.63 ± 0.08		0.70 ± 0.09	0.63 ± 0.08	
F	19.6 ± 4.4	12.0 ± 3.3		2.1 ± 2.0	1.4 ± 1.2	< 1.6	845 ± 88	36.4 ± 6.4	3.8 ± 0.4 %	3.0 ± 0.3 %	2.1 ± 0.2 %		3.0 ± 0.3 %	2.1 ± 0.2 %	
Si	38 ± 19	18.7 ± 9.6		1032 ± 515	1030 ± 515	1070 ± 535	1500 ± 750	26 ± 13	900 ± 450	1520 ± 760	72 ± 36		1520 ± 760	72 ± 36	
Ti	1615 ± 810	1580 ± 790	1010 ± 505	3.7 ± 1.9	3.1 ± 1.6	3.9 ± 1.9	1.4 ± 0.7	1.6 ± 0.8	0.44 ± 0.22	3.8 ± 1.9	0.23 ± 0.12		3.8 ± 1.9	0.23 ± 0.12	
V	1.7 ± 0.9	1.4 ± 0.7	3.2 ± 1.6	12.0 ± 6.0	10.3 ± 5.1	13.5 ± 6.8	4.2 ± 2.1	5.6 ± 2.8	9.9 ± 5.0	77 ± 38	1.3 ± 0.7		77 ± 38	1.3 ± 0.7	
Cr	7.0 ± 3.5	4.9 ± 2.5	14.3 ± 7.2	20.0 ± 10.0	10.3 ± 5.1	13.5 ± 6.8	5.9 ± 3.0	6.0 ± 3.0	0.49 ± 0.25	5.0 ± 2.5	1.0 ± 0.5		5.0 ± 2.5	1.0 ± 0.5	
Sc	7.9 ± 3.9	6.4 ± 3.2	6.7 ± 3.4	7.0 ± 3.5	7.0 ± 3.5	7.3 ± 3.7	12.5 ± 6.3	10.1 ± 5.1	18.1 ± 9.1	18.1 ± 9.1	18.0 ± 9.0		18.1 ± 9.1	18.0 ± 9.0	
Rb	10.5 ± 5.3	9.6 ± 4.8					41 ± 10	34.2 ± 8.6	61 ± 15	64.1 ± 6.4	66 ± 17		64.1 ± 6.4	66 ± 17	
Sr	37 ± 19	34 ± 19	35.0 ± 8.8	37.3 ± 9.3	36.2 ± 9.1	38.0 ± 9.5	41 ± 10	34.2 ± 8.6	61 ± 15	64.1 ± 6.4	66 ± 17		64.1 ± 6.4	66 ± 17	
Ba	0.05 ± 0.03	0.12 ± 0.03	0.29 ± 0.05	0.26 ± 0.06	0.22 ± 0.05	0.24 ± 0.07	0.15 ± 0.03	0.10 ± 0.29	0.38 ± 0.06	0.25 ± 0.04	0.44 ± 0.05		0.25 ± 0.04	0.44 ± 0.05	
Th	2.63 ± 0.31	0.93 ± 0.13	2.37 ± 0.28	2.97 ± 0.36	2.38 ± 0.29	3.46 ± 0.42	7.13 ± 0.76	7.18 ± 0.76	8.1 ± 1.0	6.80 ± 0.72	9.0 ± 1.0		6.80 ± 0.72	9.0 ± 1.0	
U	0.44 ± 0.09	0.17 ± 0.06	0.41 ± 0.08	0.50 ± 0.10	0.48 ± 0.10	0.63 ± 0.13	9.9 ± 1.1	0.89 ± 0.14	8.4 ± 1.7	9.08 ± 0.98	9.4 ± 1.0		9.08 ± 0.98	9.4 ± 1.0	

TABLE 4 (Cont.). REE and other trace-element abundances for phosphates and adjacent phases in Monument Draw (ppm wt. unless noted).

Grain	Chlorapatite #10 Pt 1	Fluorapatite #11	Whitlockite #12 Pt 1	Whitlockite #12 Pt 2	Fluorapatite #13	Whitlockite #14 Pt 1	Whitlockite #14 Pt 2	Fluorapatite #15	Whitlockite #16	Plag 1 next to Whitt. #2	Plag 2 next to Whitt. #2
EMP Point											
La	9.7 ± 1.0	27.0 ± 2.8	29.0 ± 2.9	28.6 ± 2.9	9.28 ± 0.98	30.3 ± 3.1	27.7 ± 2.8	20.9 ± 2.1	28.4 ± 2.9	0.14 ± 0.02	0.059 ± 0.012
Ce	17.5 ± 1.8	55.1 ± 5.6	69.7 ± 7.1	68.8 ± 7.0	20.7 ± 2.2	75.7 ± 7.7	68.5 ± 7.0	46.0 ± 3.7	69.2 ± 7.0	0.12 ± 0.02	0.088 ± 0.027
Pr	1.98 ± 0.21	7.55 ± 0.77	9.9 ± 1.0	9.27 ± 0.95	2.77 ± 0.30	10.9 ± 1.2	10.0 ± 1.0	6.36 ± 0.66	9.9 ± 1.0	0.012 ± 0.002	0.007 ± 0.005
Nd	7.74 ± 0.96	36.2 ± 3.7	47.2 ± 4.8	40.2 ± 4.1	11.9 ± 1.2	49.4 ± 5.0	45.3 ± 4.6	28.8 ± 2.9	45.9 ± 4.6	0.028 ± 0.007	0.047 ± 0.006
Sm	1.87 ± 0.29	1.41 ± 0.19	11.2 ± 1.2	12.9 ± 1.3	3.41 ± 0.39	14.5 ± 1.5	13.1 ± 1.4	7.10 ± 0.78	13.6 ± 1.4	0.022 ± 0.007	<0.002
Sr	1.44 ± 0.19	1.03 ± 0.11	1.67 ± 0.17	1.67 ± 0.17	0.68 ± 0.08	1.57 ± 0.17	1.56 ± 0.16	0.76 ± 0.09	1.80 ± 0.18	0.60 ± 0.06	0.92 ± 0.15
Cd	1.10 ± 0.49	1.55 ± 0.22	15.3 ± 1.6	11.8 ± 1.3	4.16 ± 0.50	15.9 ± 1.7	16.0 ± 1.7	9.64 ± 1.1	18.1 ± 1.9	<0.007	<0.020
Tb	0.14 ± 0.06	0.28 ± 0.05	3.16 ± 0.35	2.48 ± 0.28	0.85 ± 0.11	3.41 ± 0.38	3.16 ± 0.35	1.83 ± 0.22	3.51 ± 0.37	0.005 ± 0.001	<0.004
Dy	1.70 ± 0.28	1.81 ± 0.20	22.4 ± 2.3	15.9 ± 1.7	4.35 ± 0.46	22.0 ± 2.2	20.9 ± 2.1	9.30 ± 0.96	24.2 ± 2.4	0.016 ± 0.004	0.037 ± 0.025
Ho	0.38 ± 0.08	0.32 ± 0.04	4.50 ± 0.47	3.50 ± 0.36	0.87 ± 0.11	4.29 ± 0.45	4.47 ± 0.46	1.92 ± 0.21	5.49 ± 0.56	0.009 ± 0.001	0.009 ± 0.007
Er	1.22 ± 0.19	1.09 ± 0.13	16.0 ± 1.6	11.6 ± 1.2	2.94 ± 0.31	15.5 ± 1.6	14.6 ± 1.5	6.05 ± 0.63	18.6 ± 1.9	0.010 ± 0.004	<0.030
Tm	0.21 ± 0.06	0.20 ± 0.03	2.42 ± 0.25	1.87 ± 0.20	0.43 ± 0.05	2.36 ± 0.25	2.43 ± 0.25	0.78 ± 0.09	2.85 ± 0.29	<0.007	<0.054
Yb	2.10 ± 0.26	1.90 ± 0.21	22.2 ± 2.2	18.3 ± 1.9	3.76 ± 0.40	20.1 ± 2.0	19.3 ± 1.9	5.88 ± 0.62	22.1 ± 2.2	0.004 ± 0.001	0.006 ± 0.003
Lu	0.38 ± 0.07	0.29 ± 0.04	3.56 ± 0.38	2.88 ± 0.31	0.69 ± 0.09	3.27 ± 0.35	3.11 ± 0.33	1.00 ± 0.12	3.60 ± 0.38	0.002 ± 0.002	<0.007
F	1.3 ± 0.2 %	1.0 ± 0.1 %	6.4 ± 1.2	7.7 ± 1.3	3.3 ± 0.3 %	25.2 ± 3.5	19.1 ± 2.7	2.4 ± 0.3 %	12.7 ± 3.4		
Si	83 ± 42	83 ± 42	26 ± 13	20 ± 10	138 ± 69	8.4 ± 4.2 %	1.9 ± 1.0 %	795 ± 398	38 ± 19		
Ti	956 ± 480	1425 ± 710	1410 ± 705	1420 ± 710	1325 ± 660	2235 ± 1120	1535 ± 770	1435 ± 720	1412 ± 705		
V	0.65 ± 0.33	0.55 ± 0.28	1.6 ± 0.8	1.5 ± 0.8	0.04 ± 0.02	15.9 ± 8.0	2.9 ± 1.5	0.28 ± 0.14	2.2 ± 1.1		
Cr	11.9 ± 6.0	3.1 ± 1.6	6.2 ± 3.1	5.6 ± 2.8	0.78 ± 0.39	37.9 ± 19.0	28 ± 14	4.6 ± 2.3	6.5 ± 3.3		
Sc	0.10 ± 0.05	0.77 ± 0.37	6.3 ± 3.2	6.2 ± 3.1	0.76 ± 0.38	16.2 ± 8.1	7.9 ± 3.9	1.4 ± 0.7	7.5 ± 3.8	14.5 ± 3.6	6.8 ± 0.9
Rb	27 ± 14	27 ± 14	10.2 ± 5.1	10.3 ± 5.2	17.4 ± 8.7	11.7 ± 5.8	10.9 ± 5.5	18.4 ± 9.2	11.0 ± 5.5	60.2 ± 6.0	111 ± 14
Sr	119 ± 32	106 ± 27	37.6 ± 9.4	35.9 ± 9.0	64 ± 16	37.7 ± 9.5	37.6 ± 9.4	66 ± 17	39.5 ± 9.9	88.4 ± 8.8	57.0 ± 6.1
Ba	2.32 ± 0.26	1.15 ± 0.13	0.11 ± 0.03	0.12 ± 0.03	0.12 ± 0.02	0.16 ± 0.04	0.18 ± 0.04	0.24 ± 0.04	0.11 ± 0.03	34.7 ± 3.5	
Th	1.06 ± 0.13	0.93 ± 0.12	2.95 ± 0.34	1.60 ± 0.19	7.60 ± 0.80	2.22 ± 0.28	1.77 ± 0.21	6.99 ± 0.73	3.36 ± 0.38		
U	1.24 ± 0.19	1.42 ± 0.19	0.53 ± 0.09	0.32 ± 0.08	13.6 ± 1.4	0.23 ± 0.05	0.12 ± 0.03	5.41 ± 0.59	0.55 ± 0.10		
Oliv 1 next to Whitt. #2											
La	0.005 ± 0.001	0.008 ± 0.002	0.008 ± 0.002	0.015 ± 0.003	0.014 ± 0.003	0.013 ± 0.003	0.021 ± 0.005	0.014 ± 0.004	0.007 ± 0.002	0.024 ± 0.005	0.004 ± 0.001
Ce	0.011 ± 0.003	0.025 ± 0.005	0.010 ± 0.002	0.034 ± 0.006	0.027 ± 0.005	0.023 ± 0.005	0.055 ± 0.009	0.023 ± 0.006	0.008 ± 0.002	0.060 ± 0.009	0.010 ± 0.003
Pr	0.002 ± 0.001	0.008 ± 0.002	0.003 ± 0.001	0.005 ± 0.001	0.009 ± 0.003	0.005 ± 0.002	0.011 ± 0.003	0.006 ± 0.002	0.003 ± 0.001	0.009 ± 0.003	0.003 ± 0.001
Nd	0.014 ± 0.005	0.025 ± 0.006	0.020 ± 0.005	0.022 ± 0.005	0.033 ± 0.008	0.010 ± 0.003	0.010 ± 0.003	0.021 ± 0.006	0.017 ± 0.004	0.044 ± 0.009	0.017 ± 0.004
Sm	0.015 ± 0.006	0.017 ± 0.006	0.021 ± 0.007	0.009 ± 0.005	<0.007	0.016 ± 0.005	0.034 ± 0.010	0.023 ± 0.006	0.019 ± 0.007	0.019 ± 0.007	0.008 ± 0.005
Eu	0.006 ± 0.002	0.003 ± 0.002	0.003 ± 0.001	0.004 ± 0.002	0.009 ± 0.002	0.004 ± 0.002	0.005 ± 0.002	0.005 ± 0.002	0.004 ± 0.002	0.003 ± 0.002	0.005 ± 0.002
Gd	0.012 ± 0.005	0.009 ± 0.008	<0.011	0.028 ± 0.007	0.012 ± 0.008	<0.003	0.050 ± 0.014	0.021 ± 0.008	<0.005	0.028 ± 0.008	0.010 ± 0.007
Tb	0.003 ± 0.001	0.002 ± 0.001	0.002 ± 0.001	0.006 ± 0.003	0.008 ± 0.003	0.001 ± 0.001	0.007 ± 0.003	0.002 ± 0.002	0.003 ± 0.001	0.004 ± 0.001	0.001 ± 0.001
Dy	0.018 ± 0.005	0.032 ± 0.006	0.011 ± 0.004	0.022 ± 0.005	0.024 ± 0.006	0.011 ± 0.003	0.049 ± 0.009	0.016 ± 0.004	0.013 ± 0.004	0.037 ± 0.007	0.010 ± 0.003
Ho	0.007 ± 0.002	0.009 ± 0.002	0.005 ± 0.002	0.008 ± 0.003	0.007 ± 0.003	0.005 ± 0.002	0.013 ± 0.003	0.004 ± 0.002	0.004 ± 0.002	0.013 ± 0.003	0.003 ± 0.001
Er	0.018 ± 0.004	0.024 ± 0.006	0.017 ± 0.004	0.028 ± 0.008	0.020 ± 0.004	0.013 ± 0.003	0.050 ± 0.009	0.006 ± 0.004	0.010 ± 0.003	0.042 ± 0.008	0.013 ± 0.003
Tm	0.007 ± 0.002	0.007 ± 0.003	0.006 ± 0.003	0.005 ± 0.003	0.006 ± 0.003	0.003 ± 0.001	0.012 ± 0.003	0.009 ± 0.004	0.004 ± 0.002	0.005 ± 0.002	0.006 ± 0.003
Yb	0.042 ± 0.007	0.064 ± 0.009	0.038 ± 0.007	0.058 ± 0.008	0.055 ± 0.009	0.036 ± 0.006	0.100 ± 0.014	0.026 ± 0.007	0.055 ± 0.008	0.081 ± 0.012	0.061 ± 0.009
Lu	0.004 ± 0.001	0.011 ± 0.003	0.018 ± 0.004	0.015 ± 0.003	0.020 ± 0.005	0.011 ± 0.002	0.021 ± 0.005	0.012 ± 0.005	0.010 ± 0.002	0.026 ± 0.007	0.019 ± 0.004
Oliv 1 next to Whitt. #15											
La	0.005 ± 0.001	0.008 ± 0.002	0.008 ± 0.002	0.015 ± 0.003	0.014 ± 0.003	0.013 ± 0.003	0.021 ± 0.005	0.014 ± 0.004	0.007 ± 0.002	0.024 ± 0.005	0.004 ± 0.001
Ce	0.011 ± 0.003	0.025 ± 0.005	0.010 ± 0.002	0.034 ± 0.006	0.027 ± 0.005	0.023 ± 0.005	0.055 ± 0.009	0.023 ± 0.006	0.008 ± 0.002	0.060 ± 0.009	0.010 ± 0.003
Pr	0.002 ± 0.001	0.008 ± 0.002	0.003 ± 0.001	0.005 ± 0.001	0.009 ± 0.003	0.005 ± 0.002	0.011 ± 0.003	0.006 ± 0.002	0.003 ± 0.001	0.009 ± 0.003	0.003 ± 0.001
Nd	0.014 ± 0.005	0.025 ± 0.006	0.020 ± 0.005	0.022 ± 0.005	0.033 ± 0.008	0.010 ± 0.003	0.010 ± 0.003	0.021 ± 0.006	0.017 ± 0.004	0.044 ± 0.009	0.017 ± 0.004
Sm	0.015 ± 0.006	0.017 ± 0.006	0.021 ± 0.007	0.009 ± 0.005	<0.007	0.016 ± 0.005	0.034 ± 0.010	0.023 ± 0.006	0.019 ± 0.006	0.019 ± 0.007	0.008 ± 0.005
Eu	0.006 ± 0.002	0.003 ± 0.002	0.003 ± 0.001	0.004 ± 0.002	0.009 ± 0.002	0.004 ± 0.002	0.005 ± 0.002	0.005 ± 0.002	0.004 ± 0.002	0.003 ± 0.002	0.005 ± 0.002
Gd	0.012 ± 0.005	0.009 ± 0.008	<0.011	0.028 ± 0.007	0.012 ± 0.008	<0.003	0.050 ± 0.014	0.021 ± 0.008	<0.005	0.028 ± 0.008	0.010 ± 0.007
Tb	0.003 ± 0.001	0.002 ± 0.001	0.002 ± 0.001	0.006 ± 0.003	0.008 ± 0.003	0.001 ± 0.001	0.007 ± 0.003	0.002 ± 0.002	0.003 ± 0.001	0.004 ± 0.001	0.001 ± 0.001
Dy	0.018 ± 0.005	0.032 ± 0.006	0.011 ± 0.004	0.022 ± 0.005	0.024 ± 0.006	0.011 ± 0.003	0.049 ± 0.009	0.016 ± 0.004	0.013 ± 0.004	0.037 ± 0.007	0.010 ± 0.003
Ho	0.007 ± 0.002	0.009 ± 0.002	0.005 ± 0.002	0.008 ± 0.003	0.007 ± 0.003	0.005 ± 0.002	0.013 ± 0.003	0.004 ± 0.002	0.004 ± 0.002	0.013 ± 0.003	0.003 ± 0.001
Er	0.018 ± 0.004	0.024 ± 0.006	0.017 ± 0.004	0.028 ± 0.008	0.020 ± 0.004	0.013 ± 0.003	0.050 ± 0.009	0.006 ± 0.004	0.010 ± 0.003	0.042 ± 0.008	0.013 ± 0.003
Tm	0.007 ± 0.002	0.007 ± 0.003	0.006 ± 0.003	0.005 ± 0.003	0.006 ± 0.003	0.003 ± 0.001	0.012 ± 0.003	0.009 ± 0.004	0.004 ± 0.002	0.005 ± 0.002	0.006 ± 0.003
Yb	0.042 ± 0.007	0.064 ± 0.009	0.038 ± 0.007	0.058 ± 0.008	0.055 ± 0.009	0.036 ± 0.006	0.100 ± 0.014	0.026 ± 0.007	0.055 ± 0.008	0.081 ± 0.012	0.061 ± 0.009
Lu	0.004 ± 0.001	0.011 ± 0.003	0.018 ± 0.004	0.015 ± 0.003	0.020 ± 0.005	0.011 ± 0.002	0.021 ± 0.005	0.012 ± 0.005	0.010 ± 0.002	0.026 ± 0.007	0.019 ± 0.004
Oliv 1 next to Whitt. #14											
La	0.005 ± 0.001	0.008 ± 0.002	0.008 ± 0.002	0.015 ± 0.003	0.014 ± 0.003	0.013 ± 0.003	0.021 ± 0.005	0.014 ± 0.004	0.007 ± 0.002	0.024 ± 0.005	0.004 ± 0.001
Ce	0.011 ± 0.003	0.025 ± 0.005	0.010 ± 0.002	0.034 ± 0.006	0.027 ± 0.005	0.023 ± 0.005	0.055 ± 0.009	0.023 ± 0.006	0.008 ± 0.002	0.060 ± 0.009	0.010 ± 0.003
Pr	0.002 ± 0.001	0.008 ± 0.002	0.003 ± 0.001	0.005 ± 0.001	0.009 ± 0.003	0.005 ± 0.002	0.011 ± 0.003	0.006 ± 0.002	0.003 ± 0.001	0.009 ± 0.003	0.003 ± 0.001
Nd	0.014 ± 0.005	0.025 ± 0.006	0.020 ± 0.005	0.022 ± 0.005	0.033 ± 0.008	0.010 ± 0.003	0.010 ± 0.003	0.021 ± 0.006	0.017 ± 0.004	0.044 ± 0.009	0.017 ± 0.004
Sm	0.015 ± 0.006	0.017 ± 0.006	0.021 ± 0.007	0.009 ± 0.005	<0.007	0.016 ± 0.005	0.034 ± 0.010	0.023 ± 0.006	0.019 ± 0.006	0.019 ± 0.007	0.008 ± 0.005
Eu	0.006 ± 0.002	0.003 ± 0.002	0.003 ± 0.001	0.004 ± 0.002	0.009 ± 0.002	0.004 ± 0.002	0.005 ± 0.002	0.005 ± 0.002	0.004 ± 0.002	0.003 ± 0.002	0.005 ± 0.002
Gd	0.012 ± 0.005	0.009 ± 0.008	<0.011	0.028 ± 0.007	0.012 ± 0.008	<0.003	0.050 ± 0.014	0.021 ± 0.008	<0.005	0.028 ± 0.008	0.010 ± 0.007
Tb	0.003 ± 0.001	0.002 ± 0.001	0.002 ± 0.001	0.006 ± 0.003	0.008 ± 0.003	0.001 ± 0.001	0.007				

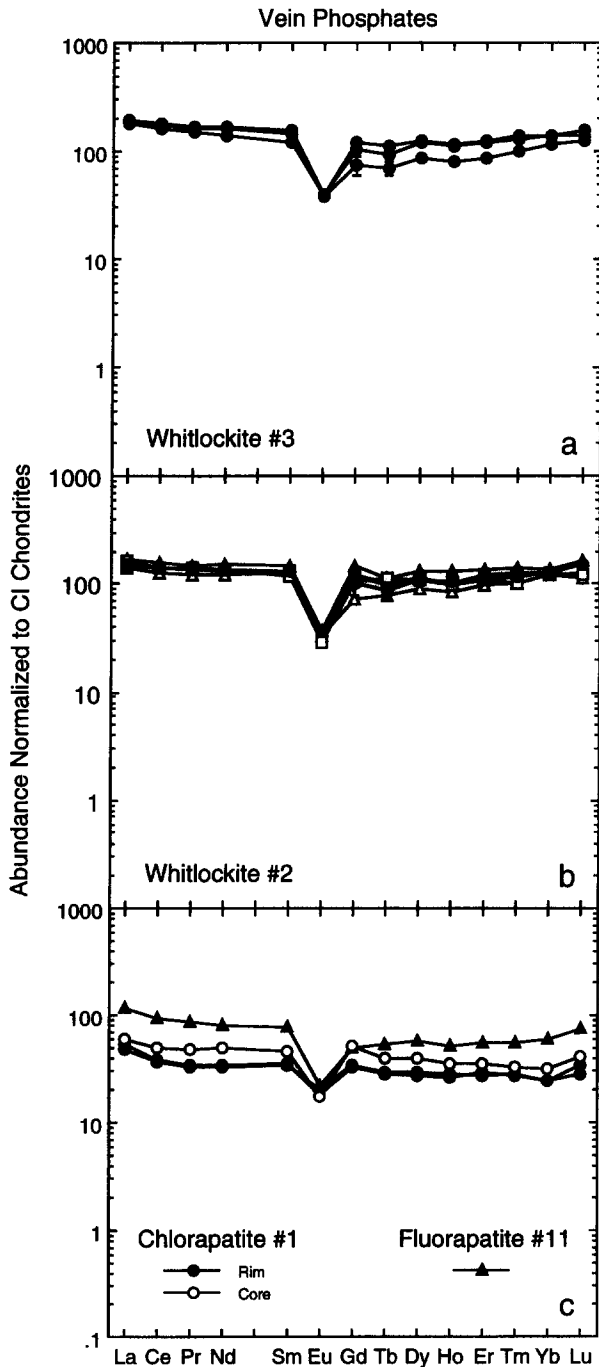


FIG. 8. REE abundances for vein phosphates from Monument Draw normalized to CI chondrites (Anders and Grevesse, 1989). (a) Three measurements of whitlockite #3, a vein-forming phosphate. 1σ relative errors are shown for one of the measurements. (b) Six measurements of whitlockite #2, which is associated with the largest Fe,Ni-FeS vein. The six measurements are essentially within uncertainties of one another (1σ errors are shown for one measurement). (c) Three measurements from chlorapatite #1 and one from fluorapatite #11, both of which are associated with the largest Fe,Ni-FeS veins. The core of chlorapatite #1 has higher REE abundances than two points near the edge. Fluorapatite #11 has higher REE abundances than chlorapatite #1, perhaps reflecting differences in partitioning between the two phases.

ment Draw define a "plateau" age of 4.517 ± 0.006 Ga. Within analytical uncertainties, the ages of Acapulco and Monument Draw are identical. The ^{39}Ar - ^{40}Ar age spectrum of Monument Draw is unusual in showing identical ages across almost the entire ^{39}Ar release. This indicates that no significant thermal event has affected this meteorite during the past 4.5 Ga.

We also examined the argon isotopic data for Monument Draw in an isochron plot of $^{40}\text{Ar}/^{36}\text{Ar}$ vs. $^{39}\text{Ar}/^{36}\text{Ar}$ (Fig. 13). All extractions define a highly linear ($r^2 = 0.99994$) isochron which passes through the origin. The age derived from the slope of a least squares fit to these data is 4.523 ± 0.005 Ga and agrees within quoted uncertainties with the plateau age of 4.517 ± 0.011 Ga. The fact that the isochron passes within uncertainty of the origin indicates the absence of any measurable excess ^{40}Ar component not associated with K.

The analytical uncertainties of ± 6 – 11 Ma quoted above for the ages of Monument Draw and Acapulco demonstrate that in favorable cases it is possible, in principle, to determine the ^{39}Ar - ^{40}Ar ages of meteorites with high precision. However, dating by ^{39}Ar - ^{40}Ar is an activation analysis technique and thus possesses an additional uncertainty parameter not present in some other chronometers. The age uncertainties quoted above do not include uncertainties in measuring neutron fluence constants, J , nor in determining the absolute age of the NL-25 hornblende fluence monitor. The uncertainties in J quoted earlier are $\pm 0.2\%$ for Acapulco and $\pm 0.8\%$ for Monument Draw and would increase the uncertainties for the ^{39}Ar - ^{40}Ar plateau ages to 4.510 ± 0.020 Ga for Acapulco and 4.517 ± 0.046 Ga for Monument Draw. However, the good agreement of ^{39}Ar - ^{40}Ar ages between Acapulco and Monument Draw, which were irradiated separately, suggests that the uncertainties associated with J values are overestimated. For absolute ages there is an additional estimated uncertainty of up to $\pm 0.5\%$ in the absolute age of the NL-25 hornblende, a topic we discuss later in greater detail.

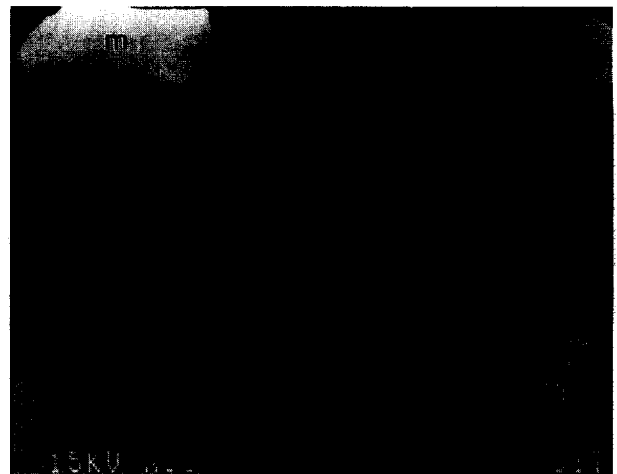


FIG. 9. Backscattered electron image of phosphate #6, surrounded by silicates (s) and metal (m). This grain consists of both apatite (a) and whitlockite (w). Ion probe pits for points #1 and #2 and for a preliminary analysis point (p) can be seen. Scale bar = 100 μm .

The ^{39}Ar - ^{40}Ar ages reported here for Monument Draw and Acapulco are identical within their relative uncertainties to ^{39}Ar - ^{40}Ar ages of 4.511 ± 0.007 , 4.519 ± 0.017 , and 4.507 ± 0.024 Ga that we recently determined for acapulcoites ALH A81261, EET 84302, and ALH A81187, respectively (Mittlefehldt et al., 1996). All five acapulcoites analyzed at JSC are consistent with a common age of 4.51 ± 0.02 Ga, where the larger error includes uncertainties associated with the absolute age of the hornblende age monitor. (Only the uncertainty associated with the Monument Draw age exceeds this error limit.) Kaneoka et al. (1992) reported slightly older ages of 4.531 ± 0.021 Ga and 4.556 ± 0.053 Ga for acapulcoites ALH 78230 and Yamato 74063, respectively.

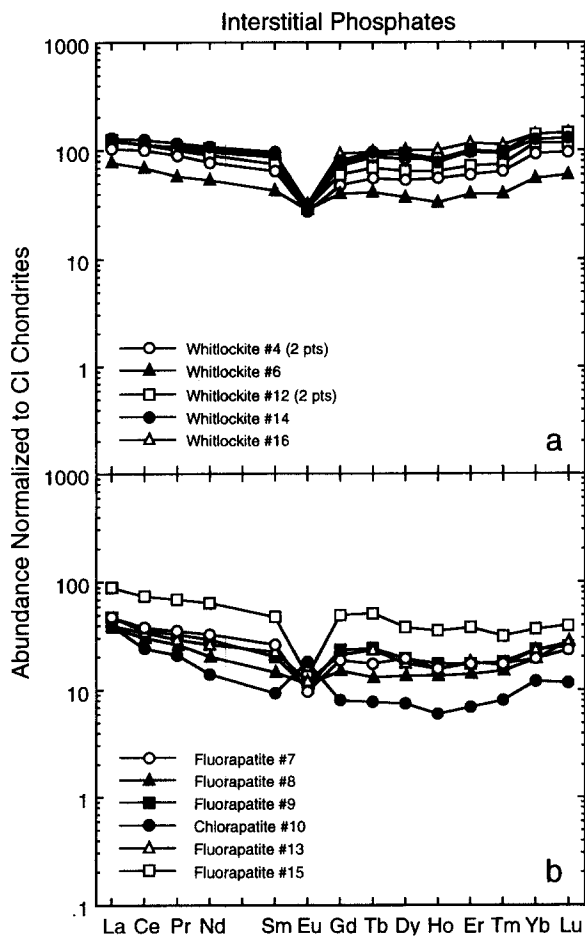


FIG. 10. CI-normalized REE abundances for interstitial phosphates from Monument Draw. (a) Whitlockites tend to have flat patterns with a negative Eu anomaly. The Eu anomaly is smaller in grains with lower REE abundances, suggesting that these grains are farther from equilibrium REE partitioning. One analysis is plotted for grains #6, and #14 because the measurements are so similar (e.g., Fig. 10b). The spread in REE abundances among the interstitial grains indicates that Monument Draw did not achieve chemical equilibrium with respect to the REEs. (b) Fluorapatites and chlorapatites are relatively enriched in LREEs and typically have a negative Eu anomaly. One grain, chlorapatite #10 has a large positive Eu anomaly and a more fractionated pattern than the other apatites. This unusual pattern and the relative large spread in the REE abundance between the grains again points to a lack of large-scale chemical equilibrium (see text).

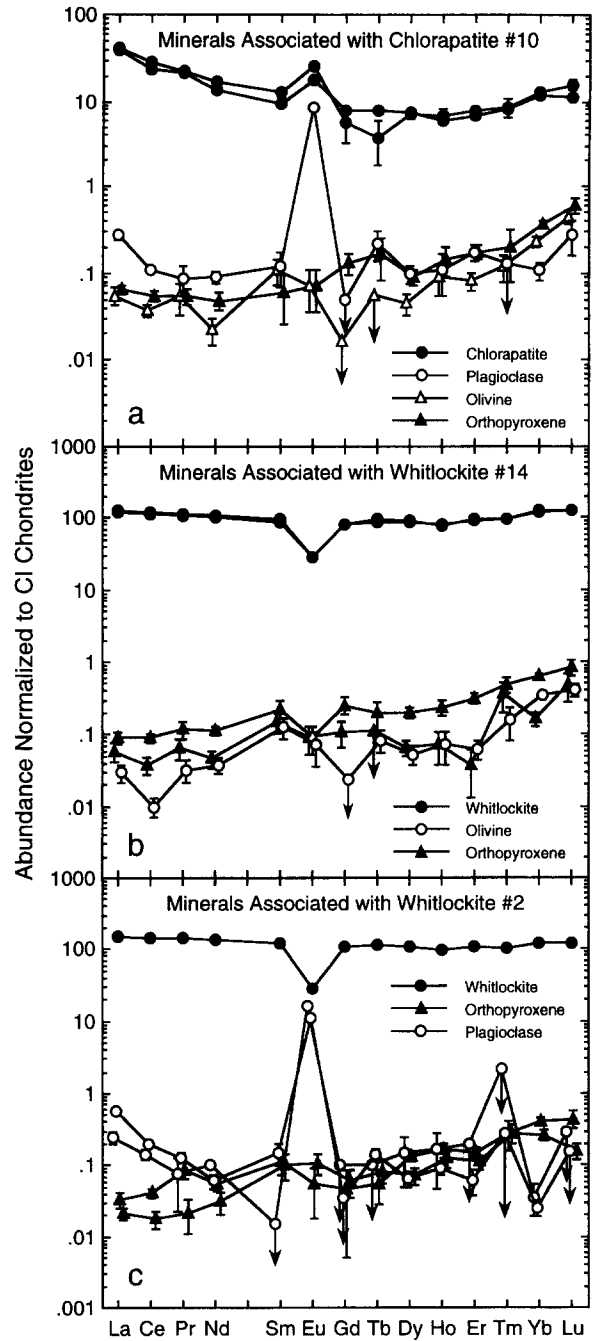


FIG. 11. CI-normalized REE abundance for phosphates and associated silicates. (a) Chlorapatite #10 and associated plagioclase, olivine, and orthopyroxene. Chlorapatite #10 is the only phosphate found to have a positive Eu anomaly. The patterns for plagioclase, olivine, and pyroxene are broadly consistent with theoretical expectations, except that the differences between REE abundances are smaller than expected. (b) Whitlockite #14 (2 measurements) and associated olivine and orthopyroxene. Again, patterns are generally consistent with expectations, but there are significant abundance differences among the orthopyroxenes and the partitioning between phosphate and silicate is not as extreme as expected. (c) Vein whitlockite #2 and associated orthopyroxene and plagioclase. This assemblage appears to be somewhat more equilibrated than those in (a) and (b), but is still not fully equilibrated (cf., Davis et al., 1993).

TABLE 5. Argon isotopic data for Acapulco and Monument Draw. Columns show extraction temperatures in °C, ³⁹Ar concentration in units of 10⁻⁴ cm³STP/g, calculated ³⁹Ar-⁴⁰Ar age in Ga, calculated K/Ca elemental ratio, and the ⁴⁰Ar/³⁹Ar, ³⁸Ar/³⁹Ar, ³⁷Ar/³⁹Ar, and ³⁶Ar/³⁹Ar ratios and their uncertainties. The 38/39 and 36/39 ratios have been multiplied by 100. All data have been corrected for radioactive decay, blanks, and reactor-produced interferences. Uncertainties shown were derived from uncertainties in these corrections and in measured ratios. Listed ages do not include an uncertainty arising from the neutron flux monitor.

Temp. °C	³⁹ Ar 10 ⁻⁴	AGE Ga	K/Ca x100	40/39	38/39 x100	37/39	36/39 x100
Acapulco							
400	0.010	----	42. ±6	-22,700	-1540	1.26 ±19	-7740
530	0.148	5.28 ±0.04	20.1 ±4.5	157 ±3	23.3 ±1.4	2.63 ±0.6	53.9 ±3.9
700	0.974	3.208 ±0.07	15.1 ±1.7	43.7 ±2	6.06 ±2.8	3.49 ±0.4	10.3 ±5.9
800	3.42	3.748 ±0.03	22.3 ±2	62.1 ±1	1.43 ±1.4	2.37 ±0.2	0.31 ±0.9
875	3.99	4.375 ±0.02	22.9 ±2	91.5 ±1	1.66 ±1.4	2.30 ±0.2	0.19 ±0.7
925	4.30	4.487 ±0.02	19.2 ±2	98.0 ±1	4.15 ±1.4	2.75 ±0.3	0.43 ±0.9
975	4.94	4.497 ±0.02	13.4 ±1	98.6 ±1	12.5 ±1.4	3.93 ±0.4	0.98 ±1.1
1025	5.02	4.510 ±0.03	9.61 ±1.0	99.4 ±2	31.2 ±0.2	5.49 ±0.6	1.33 ±1.1
1075	3.00	4.519 ±0.02	7.61 ±0.8	99.9 ±1	39.2 ±2	6.93 ±0.7	1.78 ±1.8
1200	9.27	4.506 ±0.02	3.78 ±0.4	99.1 ±1	70.5 ±2	14.0 ±1	5.78 ±1.8
1275	1.93	4.502 ±0.06	0.533 ±0.06	98.9 ±4	211 ±9	99.0 ±1.1	27.3 ±4.9
1375	0.708	4.297 ±0.14	0.271 ±0.04	87.3 ±7	92.0 ±1.0	195 ±3	142 ±2
1500	0.229	4.180 ±0.30	0.365 ±0.08	81.2 ±1.5	154 ±3	145 ±3	347 ±8
1600	0.056	2.375 ±1.66	6.52 ±8.3	24.3 ±3.1	27.1 ±6.1	8.1 ±1.0	56 ±12
Monument Draw							
400	0.014	----	9 ±13	----	2280	6.0 ±8.6	194 ±42
500	0.026	3.695 ±0.42	9.7 ±4.1	201 ±6	672 ±1	5.41 ±2.26	50.0 ±6
610	0.196	4.519 ±0.08	13.3 ±4	334 ±2	125 ±1	3.98 ±1.1	4.06 ±9.3
675	0.355	4.522 ±0.07	16.4 ±2	334 ±1	41.0 ±5	3.21 ±0.4	1.69 ±4.7
725	0.498	4.532 ±0.10	17.1 ±2	336 ±2	22.5 ±4	3.09 ±0.4	1.01 ±3.1
775	0.9528	4.516 ±0.05	17.6 ±2	333 ±1	16.8 ±2	3.00 ±0.3	0.67 ±1.9
800	0.940	4.517 ±0.03	17.8 ±2	333 ±7	14.7 ±2	2.97 ±0.3	0.57 ±1.7
850	1.28	4.524 ±0.02	16.2 ±2	335 ±5	19.7 ±2	3.26 ±0.3	0.63 ±1.6
900	0.882	4.523 ±0.04	13.9 ±1	335 ±9	22.6 ±2	3.81 ±0.4	0.74 ±2.1
950	0.634	4.520 ±0.06	6.16 ±0.7	334 ±1	119 ±6	8.57 ±0.9	4.25 ±5.6
1050	0.441	4.490 ±0.05	2.21 ±0.2	328 ±1	104 ±5	23.9 ±2.5	7.77 ±7.0
1150	1.19	4.509 ±0.05	1.88 ±0.2	332 ±1	90.5 ±5	28.1 ±3.0	9.97 ±3.0
1225	0.346	4.523 ±0.08	0.636 ±0.07	335 ±2	14 ±17	83.0 ±9.5	62.6 ±1.1
1350	0.196	4.508 ±0.14	0.327 ±0.04	332 ±3	193 ±2	161 ±2	574 ±6
1550	0.085	4.389 ±0.32	0.355 ±0.08	308 ±6	277 ±8	149 ±3	-1040

The Ar age data reported by Kaneoka et al. (1992) show greater scatter, and the ages are defined by a smaller fraction of the total ³⁹Ar release. Within their respective uncertainties, the ages reported for ALH 78230 and Yamato 74063 overlap the value of 4.51 Ga determined by us. In addition, Schultz et al. (1982) reported a classical K-Ar age of 4.50 ± 0.15 for acapulcoite ALH A77081, and Palme et al. (1981) reported a classical K-Ar age of 4.7 ± 0.3 for Acapulco. Thus, argon data on eight acapulcoites show no evidence for significant thermal heating more recently than ~4.5 Ga ago.

4.2.2. Argon diffusion and meteorite cooling history

Stepwise temperature release data can be used to determine the Ar diffusion characteristics, D/a^2 , and to constrain the thermal history of these meteorites. The release rate of ³⁹Ar and changes in K/Ca ratios with extraction temperature indicate that at least two distinct phases degassed Ar from both meteorites. We used Monument Draw to calculate values of D/a^2 because Ar release during stepwise extraction shows almost complete separation between two phases, whereas Acapulco shows greater overlap. As the Ar diffusion properties of these two phases obviously differ, we used Arrhenius plots of ³⁹Ar (Fig. 14) to evaluate the Ar diffusivity of each phase separately. Figure 14 also shows diffusion data for the release of ³⁶Ar from the low K/Ca phase. The

trend for ³⁶Ar diffusion data is generally similar to but more linear than that for ³⁹Ar from the same phase and suggests an activation energy for argon diffusion from the high-temperature phase of ~69 kcal/mol. The plot for ³⁹Ar from the high K/Ca phase (containing ~76% of the K and ⁴⁰Ar) is strongly linear (except for the first extraction which released very little ³⁹Ar), and its slope yields an activation energy for Ar diffusion of 50 kcal/mol. This difference in activation energy means that, at ~1000°C, Ar diffuses a factor of ~10³ more readily from the low-temperature, high K/Ca phase than from the high-temperature, low K/Ca phase. Acapulco shows similar, but less well-defined diffusion data. Ordinary chondrites also commonly indicate the presence of Ar in two phases with different diffusion characteristics. Turner et al. (1978), primarily emphasizing low-temperature data, reported a mean activation energy of 45 ± 17 kcal/mol for Ar diffusion in several ordinary chondrites.

From the diffusion data and activation energies determined for Monument Draw, we used the relation given by Dodson (1973) to calculate Ar closure temperatures. This is the effective temperature at which Ar diffusion from a cooling object would cease and is dependent upon Ar diffusivity and the cooling rate of the object. From the distribution of Ca in various minerals, Zipfel et al. (1995) estimated the cooling rate to be ~100 K/Ma over the temperature range of 900–1000°C. As discussed earlier, metallographic cooling

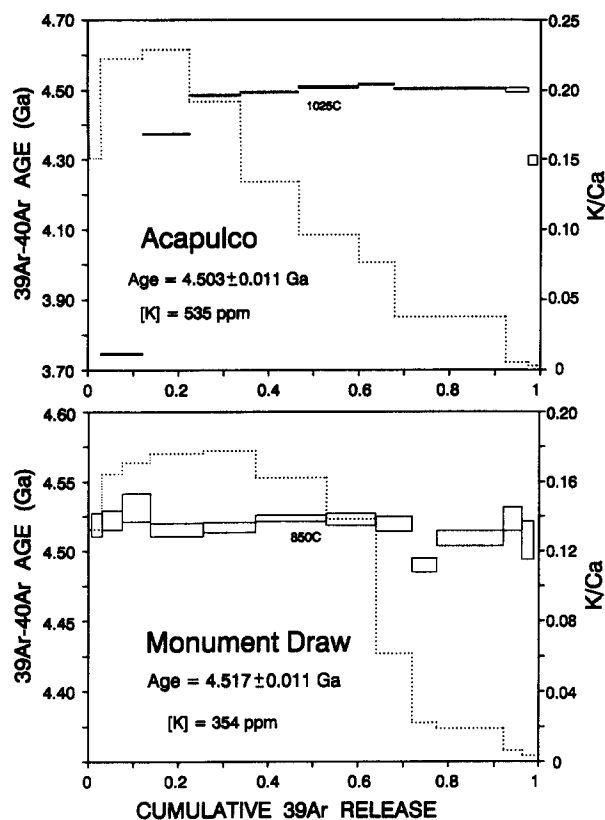


FIG. 12. ^{39}Ar - ^{40}Ar ages (rectangles) and K/Ca ratios (dotted lines) as a function of cumulative release of ^{39}Ar for stepwise extractions of (a) Acapulco and (b) Monument Draw. Individual age uncertainties are indicated by the widths of the rectangles. K concentrations and the temperature releasing 50% of the total ^{39}Ar are also indicated.

rates for the temperature interval of ~ 350 – 600°C are faster at $\sim 10^3$ – 10^5 K/Ma. For the low-temperature phase of Monument Draw, the Ar closure temperatures for the slower (100 K/Ma) and faster (0.1 K/a) cooling rates would be ~ 300 and $\sim 400^\circ\text{C}$, respectively. For the high-temperature phase, these closure temperatures would be ~ 500 and $\sim 640^\circ\text{C}$, respectively. All of these closure temperatures are considerably less than the metamorphic temperatures for these acapulcoites of ~ 950 – 1000°C . This would indicate that diffusive loss of radiogenic ^{40}Ar occurred readily during much of the period of metamorphism of the acapulcoite parent body.

Closure temperatures for Ar diffusion and the ^{39}Ar - ^{40}Ar age profiles can be used to place some constraints on the cooling history of acapulcoites. We define the cooling time as the time required for these meteorites to cool from the peak metamorphic temperature of $\sim 1000^\circ\text{C}$ to the Ar closure temperature. Figure 15 shows that this cooling time varies inversely with the assumed cooling rate, with different trend lines for the different closure temperatures calculated for the two K/Ca phases. For a cooling rate of 10 K/Ma these cooling times would be ~ 70 and ~ 50 Ma for the low-K/Ca and high-K/Ca phases, respectively. If these meteorites cooled slowly, then we would expect to see a difference in ^{39}Ar - ^{40}Ar age between their low- and high-temperature

phases because of the different cooling times to Ar closure. This difference in cooling time between phases, which is the separation between the trend lines for the two phases in Fig. 15, is shown separately as the curved line and the right-hand scale. This curved trend gives the expected difference in ^{39}Ar - ^{40}Ar age between K/Ca phases as a function of cooling rate. Examination of the ^{39}Ar - ^{40}Ar age profiles for these meteorites (Fig. 12) indicates that the ages of the two K/Ca phases are the same within about 20 Ma. This observation would restrict the cooling rate for these acapulcoites to those values which give an age difference between meteorite phases that are no greater than ~ 20 Ma. From Fig. 15, we see that the average cooling rates for these meteorites, from a temperature of $\sim 1000^\circ\text{C}$ to Ar closure, is restricted to values faster than ~ 10 K/Ma. The ^{39}Ar - ^{40}Ar data do not rule out a complex cooling history, so long as the average cooling rate was faster than ~ 10 K/Ma during the time that Ar diffusive loss occurred.

4.3. Noble Gases

4.3.1. Cosmic ray exposure age

The concentrations of cosmogenic ^3He and ^{21}Ne and the shielding parameter ($^{22}\text{Ne}/^{21}\text{Ne}$)_{cos} are given in Table 6. The ($^{22}\text{Ne}/^{21}\text{Ne}$)_{cos} ratio indicates a very low shielding of a few centimeters and, thus, probably a small pre-atmospheric size of Monument Draw. With the nuclide production model of Graf et al. (1990b), we estimate a shielding-corrected ^{21}Ne exposure age of about ~ 6.8 – 7.3 Ma. This calculation assumes an H chondritic chemical composition, which is appropriate in view of the contents (in wt%) of Mg (~ 13.3), Al (~ 1.3), Si (~ 17.8), and Fe (~ 26.0) for Monument Draw calculated from modes and mineral compositions.

^3He and ^{21}Ne _{cos} concentrations in Monument Draw are between ~ 10 – 30% lower than the respective values in four Acapulco analyses reported by Palme et al. (1981) and Evans et al. (1982). Since the Acapulco samples have somewhat lower ($^{22}\text{Ne}/^{21}\text{Ne}$)_{cos} ratios than Monument Draw, higher production rates have to be used, however. With the Graf et al. (1990b) model, and the additional reasonable assumption that the preatmospheric radius of Acapulco did not exceed 30 cm, we deduce a ^{21}Ne exposure age of ~ 7 – 8 Ma for three of the four samples, and ~ 9 – 10 Ma for the fourth one (the lower ages of ~ 4.5 Ma reported originally are due to the higher production rates used at that time). Three of the four Acapulco exposure ages are thus very similar to that of Monument Draw. Exposure ages of two other acapulcoites are also quite similar to those of Monument Draw and Acapulco. For Yamato 74063, Takaoka and Yoshida (1991) calculate a ^{21}Ne exposure age of 6.2 ± 0.6 Ma, whereas the Graf et al. (1990b) model yields ~ 6.7 Ma. Schultz et al. (1982) report for ALH A77081 a ^{21}Ne _{cos} concentration of 0.90×10^{-8} cm³STP/g and a very high ($^{22}\text{Ne}/^{21}\text{Ne}$)_{cos} ratio of 1.285. Assuming L chondrite composition for this meteorite, which is appropriate in view of the Mg concentration given by Schultz et al. (1982), we deduce a ^{21}Ne exposure age of ~ 5.2 Ma from the Graf et al. (1990b) model, almost identical to the 5.6 Ma deduced by Schultz et al. (1982) using the model of Nishiizumi et al. (1980).

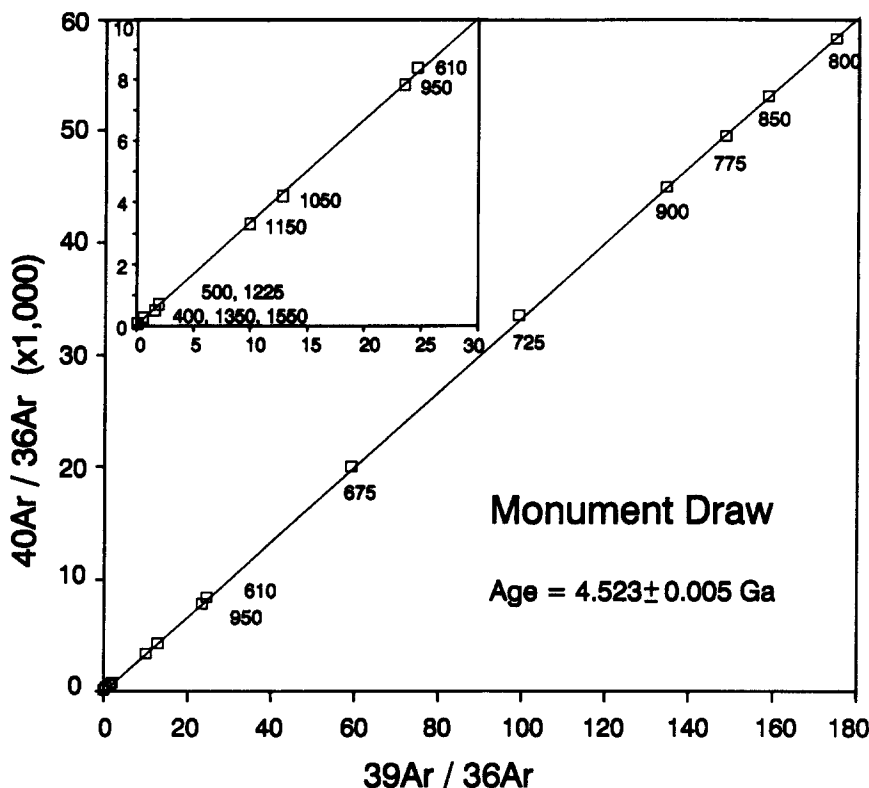


FIG. 13. Isochron plot for Monument Draw. All extractions define a highly linear ($r^2 = 0.99994$) isochron which passes through the origin. The age of 4.523 ± 0.005 Ga agrees within quoted uncertainties with the plateau age of 4.517 ± 0.011 Ga. The fact that the isochron passes within uncertainty of the origin indicates the absence of any excess ^{40}Ar component not associated with K.

4.3.2. Trapped noble gases

Monument Draw contains relatively large amounts of trapped Ar, Kr, and Xe, comparable to those in type 4 ordi-

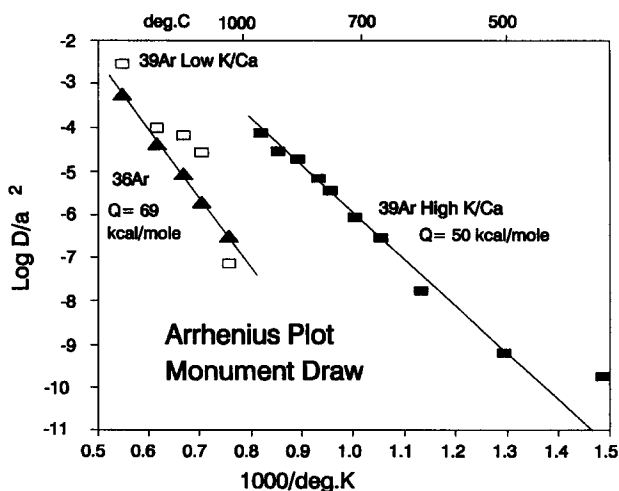


FIG. 14. Arrhenius plots for the release of ^{39}Ar from the high and low K/Ca phases of Monument Draw (low- and high-temperature, respectively), and for the release of ^{36}Ar from the low K/Ca phase. Activation energies derived for the high and low K/Ca phases are 50 kcal/mol and ~ 69 kcal/mol, respectively. At 1000°C , the rate of argon diffusion from these two phases differs by a factor of $\sim 10^3$.

nary chondrites (Table 6). In this respect, Monument Draw is similar to Acapulco (Palme et al., 1981), ALH A77081 (Schultz et al., 1982), and also to Lodran (Eugster and Weigel, 1993). The isotopic composition of trapped Ar cannot be determined, due to the presence of cosmogenic Ar, but Kr and Xe are barely influenced by cosmogenic gases. Trapped Xe in Monument Draw shows the isotopic signature Xe-Q (Wieler et al., 1991), the Xe component in carbonaceous chondrites which resides in the oxidizable carbonaceous carrier "Q." The same Xe component has also been found in ordinary chondrites (e.g., Lavielle and Marti, 1992), in Lodran (Eugster and Weigel, 1993), and in the acapulcoite Yamato 74063 (Takaoka et al., 1993). The isotopic composition of Kr in Monument Draw is not identical to that of Kr-Q, unlike the case in Lodran and Yamato 74063. Rather, it is enriched relative to Kr-Q by $\sim 4\%$ in ^{82}Kr and by $\sim 1.5\%$ in ^{86}Kr , but depleted by $\sim 2.5\%$ in ^{83}Kr . This composition cannot be explained by mass-fractionated solar Kr or Kr-Q nor by addition of cosmogenic or fissionogenic Kr to such mass-fractionated trapped Kr.

4.3.3. Element ratios Ar/Kr/Xe

In Monument Draw, both Ar/Xe and Kr/Xe are about 2–3 times lower than in phase Q in Allende or Murchison. Whereas $^{36}\text{Ar}/^{132}\text{Xe}$ as low as ~ 30 as in Monument Draw is sometimes observed in H chondrites (e.g., Loeken et al.,

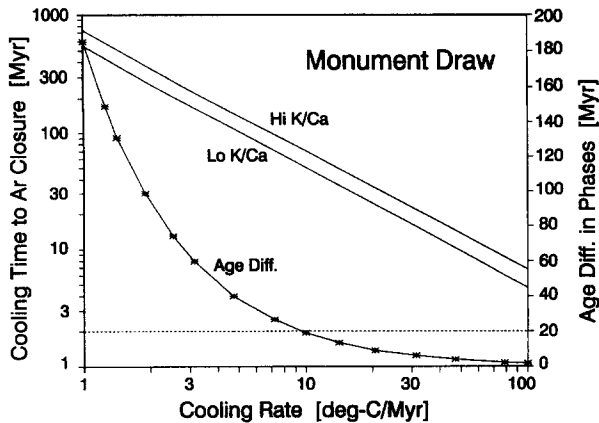


FIG. 15. Plot of cooling times (straight lines and left-hand scale) from 1000°C to closure of the K–Ar chronometer as a function of cooling rate (in K/Ma) for the two K-bearing phases of Monument Draw. With increasing cooling rates, the closure temperature to Ar diffusion increases, whereas the cooling time to closure decreases. The two K/Ca phases show different cooling trends because of differences in Ar diffusion properties and thus Ar closure temperatures. The curved line and right-hand scale show the difference in cooling times (in Ma) between the two cooling curves for high and low K/Ca phases; this difference decreases with faster cooling rates. Figure 11 suggests a maximum age difference between the two Monument Draw phases of ~ 20 Ma, which is the horizontal dotted line. This dotted line intersects the curved, age difference line at a cooling rate of ~ 10 K/Ma. Thus, from its peak temperature of $\sim 1000^\circ\text{C}$ to the Ar closure temperature, Monument Draw must have cooled at an average rate faster than 10 K/Ma.

1992), the $^{84}\text{Kr}/^{132}\text{Xe}$ ratio in Monument Draw of only ~ 0.36 is remarkably low.

5. DISCUSSION

The data summarized above, both new and previously published data, allow us to outline the history of the acapulcoite parent body. We are interested primarily in four aspects of this history: (1) the properties of the precursor chondritic material, (2) the nature of the heating (e.g., peak temperature, heat source, cooling rate) inferred from petrology and major element chemistry, (3) the history of the acapulcoites inferred from trace elements, and (4) the chronological history of the acapulcoites, including inferences for the thermal history and sampling of the acapulcoite parent body as deduced from cosmic ray exposure ages. A fifth aspect, the high abundance of trapped noble gases, is treated briefly at the end of the discussion.

5.1. Precursor Chondrite

The roughly chondritic mineralogy and mineral abundances of all acapulcoites and the presence of relict chondrules in Monument Draw and Yamato 74063 provide strong evidence that the precursor rock of the acapulcoites was chondritic. However, this material was unlike any known chondrite, as is indicated by mafic mineral compositions which are intermediate between those of ordinary and enstatite chondrites, and by oxygen isotopic compositions which are unlike those of ordinary and enstatite chondrites. The

carbonaceous CR chondrites and Kakangari have oxygen isotopic compositions similar to those of the acapulcoites, although the former exhibit a much larger range. This, in addition to the lower FeO contents of olivine in Kakangari (Fa_{1-4} ; Brearley, 1989), suggests that the oxygen isotopic similarities are a coincidence and do not imply a relationship between acapulcoites and these carbonaceous meteorites.

5.2. Thermal History Derived from Petrology

5.2.1. Peak temperature

The equigranular textures, abundant 120° triple junctions, large plagioclase grains, and rare and highly recrystallized relict chondrules of acapulcoites suggest that these rocks were extensively heated on their parent body. Comparison to textures of type 6 ordinary chondrites indicates that the peak temperatures were at least $\sim 750\text{--}950^\circ\text{C}$ (Dodd, 1981). Although absolute temperature estimates from two-pyroxene geothermometry have considerable uncertainties, the values obtained for acapulcoites of $980\text{--}1170^\circ\text{C}$ suggest that heating was to temperatures in excess of the Fe,Ni–FeS cotectic of about 980°C (Kullerud, 1963; Kubaschewski, 1982). This cotectic melt consists of 85 wt% FeS and 15 wt% Fe,Ni and is the first partial melt in a chondritic system. Evidence for partial melting at the cotectic exists in the form of micrometer-sized veins dominated by FeS in all acapulcoites and millimeter- to centimeter-sized veins of Fe,Ni–FeS in Monument Draw. Temperatures were apparently sufficiently high to mobilize phosphates which are found in phosphate veins and associated with the Fe,Ni–FeS veins. The detailed melting behavior of phosphates in these multicomponent systems has not been studied. However, phosphates are observed as late-crystallizing phases in a variety of igneous rocks, including eucrites and SNCs, and should therefore be early melting phases. Thus, we conclude that acapulcoites were heated in excess of 950°C , where Fe,Ni–FeS cotectic melting occurred and Fe,Ni metal, troilite, and phosphates were mobilized. We would note, however, that acapulcoites do not contain equal abundances of these Fe,Ni–FeS veins and, thus, may not have reached identical peak temperatures. It is possible that the vein-rich Monument Draw was heated slightly higher than the remaining acapulcoites and, thus, had more Fe,Ni–FeS melting and an increased abundance of these veins. Alternatively, the abundance of veins may not reflect differences in local heating and melting, but rather reflect the efficiency of melt migration. The physical details of melt migration in acapulcoites will be addressed in a separate paper (McCoy et al., 1996b).

Partial melting of silicates in a chondritic system begins around 1050°C , and the partial melt is roughly basaltic (plagioclase–pyroxene) in composition. However, we see no evidence for silicate partial melting in the acapulcoites. In fact, Fe,Ni–FeS veins, which start forming around $\sim 980^\circ\text{C}$, sometimes cross-cut plagioclase in Monument Draw, Acapulco, ALH A81187, and ALH A84190. This suggests that plagioclase was solid during formation of the Fe,Ni–FeS veins and, thus, temperatures did not reach those required for silicate partial melting.

Our suggestion that acapulcoites experienced no silicate

TABLE 6. Noble Gases in Monument Draw.

³ He	⁴ He	²⁰ Ne	²⁰ Ne/ ²² Ne	²² Ne/ ²¹ Ne	³⁶ Ar	³⁶ Ar/ ³⁸ Ar	⁴⁰ Ar	Cosmogenic Fraction		
								²¹ Ne	³⁸ Ar	²² Ne/ ²¹ Ne
9.52	3640	1.42	0.883	1.252	3.33	4.27	3420	1.28	0.173	1.235
<i>0.4</i>	<i>140</i>	<i>0.06</i>	<i>0.004</i>	<i>0.006</i>	<i>0.12</i>	<i>0.02</i>	<i>140</i>			
		⁸⁴ Kr						Trapped Fraction		
		<i>80/84</i>	<i>82/84</i>	<i>83/84</i>	<i>86/84</i>			³⁶ Ar/ ¹³² Xe	⁸⁴ Kr/ ¹³² Xe	
		⁸⁴ Kr=100								
		0.0397	3.93	20.96	19.86	31.48			28.9	0.355
		<i>0.0024</i>	<i>0.03</i>	<i>0.14</i>	<i>0.10</i>	<i>0.06</i>			2.3	<i>0.018</i>
		¹³² Xe								
		<i>124/132</i>	<i>126/132</i>	<i>128/132</i>	<i>129/132</i>	<i>130/132</i>	<i>131/132</i>	<i>134/132</i>	<i>136/132</i>	
		¹³² Xe=100								
		0.112	0.471	0.413	8.224	129.4	16.26	82.28	38.22	31.74
		<i>0.008</i>	<i>0.005</i>	<i>0.005</i>	<i>0.020</i>	<i>0.3</i>	<i>0.06</i>	<i>0.07</i>	<i>0.11</i>	<i>0.08</i>

Noble gas concentrations in 10⁻⁸cm³STP/g

Sample Mass: 119 mg

Stated errors (1σ, in italics) do not include uncertainty of mass discrimination.

Add 0.2% to obtain absolute errors of isotope ratios.

partial melting is in contrast to that of Zipfel et al. (1995) who suggest peak temperatures of ~1200°C for Acapulco, with partial melting of ~20% of the bulk rock. Their peak temperature estimate of 1200°C is primarily based on the chemical composition and modes of Fe,Ni-FeS blebs contained in the cores of orthopyroxene and olivine (see discussion below). These authors argue that the Ni/Ir ratios of the blebs (which differ significantly from the interstitial metal), their nonchondritic Fe,Ni / FeS ratio, and their absence from clinopyroxene grains all argue for silicate partial melting. The blebs formed by precipitation on the surfaces of residual solid grains and were trapped by bleb-free overgrowths. We find arguments concerning Fe,Ni/FeS ratios unconvincing, given the heterogeneity in Fe,Ni/FeS ratios within individual bleb-bearing mafic silicate grains (Zipfel et al., 1995) and the large uncertainties in estimating the original Fe,Ni/FeS ratio of the precursor chondrite. In addition, these blebs do not themselves outline pre-existing grains in thin section. Zipfel and Palme (1993) and Zipfel et al. (1995) argue that mechanical segregation of chromite, metal and troilite occurred, explaining the highly variable Cr abundances among acapulcoites. However, Takahashi (1983) found that even dense metal and sulfide did not segregate efficiently until 50% partial melting was exceeded. Since Cr occurs predominantly in minor phases such as chromite and chromian diopside, we suggest that the Cr variability from sample to sample of a given acapulcoite observed by Zipfel and Palme (1993) is due to heterogeneous distribution of coarse-grained phases and analysis of unrepresentatively small bulk rock samples of 100–300 mg. As an example, a 300 mg sample containing a trace of chromite (0.1%) would contain only ~12 chromite grains of 200 μm diameter. Thus, inclusion of a few more or a few less chromite grains might substantially alter the chromite budget of the sample. Finally, we question how Acapulco could retain its relatively fine-grained equigranular texture during 20% silicate partial melting. Although Zipfel et al. (1995) invoke melting in a closed system without melt migration, they provide no plausible mechanism for how this occurred. There is clear evidence in the related lodranites for up to 20% partial melting. Lo-

dranites which experienced ~20% partial melting (e.g., Lodran) have experienced substantial loss of these partial melts and are much coarser grained than acapulcoites (McCoy et al., 1996a), owing to the higher diffusion rates in silicate melts when compared to grain boundary diffusion. Thus, while we cannot unequivocally eliminate the possibility of silicate melting in Acapulco, we find silicate partial melting unlikely, particularly partial melting up to 20%.

5.2.2. Heat source

Previous investigators (Kallemeyn and Wasson, 1985; Takeda et al., 1993) have invoked collisional impact heating as the heat source for the thermal metamorphism of the acapulcoite parent body. However, we find no evidence for collisional heating and, therefore, suggest that the heat source must have been noncollisional (e.g., ²⁶Al, electromagnetic induction). Kallemeyn and Wasson (1985) argued that the textures and compositions of Acapulco and ALH A77081 resulted from brief, incomplete heating, possibly the result of impact-induced shock. Takeda et al. (1993) proposed a planetesimal collision model in which shock and the resultant heating account for the features of primitive achondrites, including acapulcoites. These authors do acknowledge that ²⁶Al may have been an additional heat source. In our view, neither of these proposals can account for the observed properties of acapulcoites. In impact events, most of the energy is partitioned into ejecting debris and brecciating the target rocks (e.g., Melosh, 1989) and, in the case of the relatively small asteroids, little melting takes place and what melt is produced is largely ejected from the asteroid (e.g., Stöffler et al., 1991). Since none of the acapulcoites are breccias nor show evidence for significant shock (they are unshocked or very weakly shocked, stage S1 to S2 of Stöffler et al., 1991), impact as the heat source seems ruled out. Furthermore, in impact events, some of the energy is partitioned into localized heating which causes formation of melt veins and shock melts (e.g., Keil et al., 1977, 1992), which are not observed in acapulcoites. We do not think that these features (brecciation, melt veins, localized melting), could

have been totally annealed out, since surely chondrules which are found as relicts in acapulcoites, would be more readily annealed out than shock veins and brecciation. In this connection, it is important to point out that the Fe,Ni-FeS-(phosphate) veins we observed are not melt veins produced by shock but, rather, were formed by heating of the rocks unaccompanied by shock. The veins we observe consist exclusively of metallic Fe,Ni-FeS and phosphates. In contrast, shock veins are total rock melts and contain melt of mafic silicates in addition to metallic Fe,Ni-FeS melts (e.g., Keil et al., 1977, 1992; Stöfler et al., 1991), a feature that is lacking in the veins in acapulcoites. In addition, in acapulcoites, Fe,Ni-FeS veins are found primarily along grain boundaries. In contrast, shock-produced melt veins cross-cut grains and show little preference to occur along grain boundaries (e.g., Keil et al., 1977, 1992). Veins very similar to those observed in acapulcoites have been produced experimentally by heating the Krymka (L3) chondrite for 1 week at 100°C temperature increments from 400–1000°C in a low-pressure environment (Ikramuddin et al., 1977). McSween et al. (1978) examined these samples and reported Fe,Ni-FeS filling grain boundaries in the 900°C experiment. Our examination of the 900°C sample revealed that the Fe,Ni-FeS veins are very similar to those in acapulcoites, particularly ALH A81187/84190. These veins are typically 1–3 μm in width and tens of micrometers in length. They occur preferentially along grain boundaries, but also cross-cut silicates. They are dominated by troilite, but some contain Fe,Ni-FeS and others are seemingly made only of Fe,Ni metal, just like those in acapulcoites; no veins of phosphates were observed in the artificially heated Krymka. The similarities between the Fe,Ni-FeS veins produced by heating and those in acapulcoites provide additional strong evidence that the veins in acapulcoites were produced by heating and not as a result of shock-melting. A full discussion of the potential noncollisional heat sources (e.g., ^{26}Al ; ^{60}Fe ; electromagnetic induction; long-lived K, U and Th) for melting is beyond the scope of this paper. However, Bernius et al. (1991) measured an upper limit for $^{26}\text{Al}/^{27}\text{Al}$ in Acapulco of 1.5×10^{-7} , suggesting that ^{26}Al could not have been the lone heat source.

An enigmatic feature of acapulcoites are blebs of mostly metallic Fe,Ni and minor FeS and phosphates that occur in the cores of mafic silicates (mostly orthopyroxene), whose origin is not understood. It seems almost certain that these blebs have an igneous origin, as also suggested by Zipfel et al. (1995). This origin could have been during melting related to shock, partial melting on the parent body, or during chondrule formation. These blebs have been attributed to an origin by shock, by analogy with blebs in the diogenite Yamato 74013 (Takeda et al., 1993, 1994). These authors did not, however, note the occurrence of the ubiquitous Fe,Ni-FeS veins. However, it appears to us that a shock model for the origin of the Fe,Ni-FeS blebs is problematic: The blebs in acapulcoites do not occur in parallel rows (with the exception of the smallest blebs in ALH A81187/84190), as do those in the diogenite, where they appear to decorate annealed planar fractures. In addition, it is not clear why shock-produced blebs should only occur in the cores of silicates and not in the rims. As discussed above, Zipfel et al. (1995)

argued that these blebs were trapped on the surfaces of residual grains during crystallization of partial melts. Schultz et al. (1982) observed that bleb-containing mafic silicates occur in semicircular outlines and suggested that they may have formed during crystallization of mafic silicates in chondrules whose outlines are now largely obscured by recrystallization. They argued that these grains may then have acquired bleb-free overgrowths during subsequent recrystallization and metamorphic grain growth. This model has appeal, but we wonder why then such bleb-bearing mafic silicates are not more common in chondritic meteorites. Note that many chondrites do contain “dusty” olivines with micrometer-sized low-Ni metal blebs inside olivine. The blebs, however, were formed by reduction of FeO in the host olivine and clearly differ from the Fe,Ni-FeS blebs found in acapulcoites. None of these models is completely satisfactory, and the origin of these blebs remains unresolved.

5.2.3. Cooling history

Our metallographic data add to a growing base of cooling rates in acapulcoites, although most of the relevant data is from Acapulco itself. Here we explore some possible interpretations of this data base and how our data influences this discussion. Very little data is available to constrain the high temperature cooling history of acapulcoites. Zipfel et al. (1995) used Ca distribution among orthopyroxene, chromian diopside, and olivine to suggest a cooling rate of ~ 100 K/Ma at $\sim 900^\circ\text{C}$. No comparable calculations from other acapulcoites exist.

At least two datasets, including our metallographic data, can be used to infer cooling at intermediate temperatures. Zipfel et al. (1995), based on Ca zoning in olivine and using new diffusion coefficients, suggested a cooling rate of 800–1000 K/Ma around 650°C , suggesting a complex cooling history. Alternatively, these authors suggested that this zoning could reflect phosphate formation and, thus, not provide meaningful cooling rate information. Our metallographic cooling rates of $10^3 - 10^5$ K/Ma for several acapulcoites also suggest rapid cooling in the temperature interval from ~ 600 – 400°C . Recently, El Goresy et al. (1995) observed graphite veneers at kamacite-taenite boundaries and suggested that these veneers may act as diffusion barriers and, thus, metallographic cooling rates might not be valid. We find this interpretation unlikely. While graphite might certainly act as a boundary, we suggest that these veneers likely formed at temperatures below that at which taenite compositions were established. The most convincing argument for this is the marked zonation within taenite. If the graphite had acted as a diffusion barrier and cooling were actually quite slow (e.g., 1–10 K/Ma), taenite would have homogenized, which it did not. This supports the idea of rapid cooling during metal exsolution.

Finally, some information is available about the low temperature cooling history of Acapulco. Pellas and Fiéni (1992) used differences in densities of Pu fission tracks between merrillite and orthopyroxene to determine a cooling rate of ~ 1.7 K/Ma over the temperature interval 290 – 110°C . This would suggest a return to slow cooling at low temperature. A second dataset may be available which would also

indicate slow cooling at low temperature. The island phase metallographic technique was utilized by Marti et al. (1994) to infer a cooling rate of 20 ± 5 K/Ma for Acapulco. While this is a metallographic technique, it may not record the same temperature range recorded by the classic metallographic technique. Haack and Rasmussen (1994) have argued that this technique records the cooling rate at temperatures below $\sim 330^\circ\text{C}$.

The acapulcoites probably experienced a complex cooling history, as also inferred by Zipfel et al. (1995). However, the full extent and cause of this complexity is unclear. The available data implies a history of moderate cooling (~ 100 K/Ma) at $\sim 900^\circ\text{C}$, followed by rapid cooling ($>10^3$ K/Ma) at $600\text{--}400^\circ\text{C}$, and slow cooling (<20 K/Ma) below 300°C . It is possible that one or more of these datasets is in error and this complex cooling is an artifact of the limited dataset. The fact that most of this data comes from Acapulco suggests that broadening the database to other acapulcoites should be a priority. Another alternative is that this cooling reflects a complex physical history of the acapulcoite parent body. Keil et al. (1994) have argued that many meteorite parent bodies experienced collisional breakup and gravitational re-assembly. This process could produce a complex cooling history with slow cooling in the original parent body, rapid cooling of the fragments (500 m to 6 km in diameter as indicated by the metallographic cooling rates; Haack et al., 1990) and slow cooling after gravitational reassembly of the parent body. It is possible that the acapulcoite parent body experienced such a complex history. A possible argument against parent body breakup is the lack of shock features in acapulcoites. However, it seems unlikely that such a process would necessarily induce shock effects in the fragments. The presence of unshocked meteorites in our collections attests to the ability to break fragments from large parent bodies without inducing shock effects. Only future cooling rate studies will be able to decide between these options.

Another apparent feature of these data is that acapulcoites experienced a range of cooling histories. While all acapulcoites may have experienced a three stage cooling history, metallographic data suggests that each acapulcoite might have cooled at a different rate during the intermediate stage. It is during this temperature interval ($600\text{--}300^\circ\text{C}$) that much of the chemical zoning might have been established by incomplete equilibration and/or reduction. Thus, the differences in zoning among acapulcoites discussed above probably reflects these somewhat different thermal histories.

5.3. History Inferred from REE Distributions

Qualitatively the phosphates in acapulcoites have REE patterns resembling those in phosphates in ordinary chondrites (Curtis and Schmitt, 1979; Crozaz and Zinner, 1985; Crozaz et al., 1989). However, there seems to be more variability in both the REE abundances and patterns among the phosphates in acapulcoites compared to phosphates in ordinary chondrites (cf. Crozaz et al., 1989). Detailed studies of REE distributions in phosphates and silicates have been carried out for Acapulco (Davis et al., 1993; Zipfel et al., 1995), ALH A81261 (Davis et al., 1993), and Monument Draw (this paper). These studies show (1) variable REE

abundances among phosphates of the same mineralogy within each meteorites and (2) different degrees of REE enrichment in phosphates relative to CI abundances. In addition, Monument Draw exhibits variable REE abundances in silicates and REE patterns incompatible with equilibrium partitioning of REE (Figs. 10 and 11). Systematically higher REE abundances are observed in whitlockite relative to apatite (Fig. 10; Davis et al., 1993; Zipfel et al., 1995), consistent with expectations based on equilibrium partitioning. At equilibrium, the LREE abundances in whitlockite should be about a factor of five higher than in apatite (e.g., Murrell et al., 1984; Davis et al., 1993). However, in general, the REE abundance differences between whitlockite and apatite in acapulcoites do not achieve this value (Fig. 10; Zipfel et al., 1995). Whitlockites from Acapulco have REE abundances ranging up to $\sim 500\times$ CI, those in ALH A81261 have REE abundances of $\sim 250\times$ CI (Davis et al., 1993; Zipfel et al., 1995), while whitlockites in Monument Draw have REE abundances from $75\text{--}200\times$ CI (Figs. 8 and 10). Davis et al. (1993) interpreted the abundance differences between whitlockites in Acapulco and ALH A81261 along with smaller than expected differences in partitioning between whitlockites and silicates as evidence that REEs in ALH A81261 were less equilibrated than in Acapulco. Monument Draw has somewhat smaller degrees of partitioning and less fractionated REE patterns, consistent with a lower degree of equilibration. Thus, there is evidence for disequilibrium in the REE distributions in all acapulcoites that have been carefully studied and Monument Draw appears to be further from equilibrium than the other two, particularly Acapulco.

These data combined with other petrologic and chemical data imply two things about the history of the acapulcoites. First, individual meteorites have apparently experienced different time/temperature histories. Acapulco seems to be the most equilibrated, ALH A81261 somewhat less equilibrated, and Monument Draw the least equilibrated. Second, the REEs in phosphates from all of the acapulcoites seem to be less equilibrated than those in ordinary chondrites, which presumably have seen lower metamorphic temperatures. Zipfel et al. (1995) recognized many of these indicators of disequilibrium in Acapulco and proposed a late-stage infiltration of a fluid phase enriched in incompatible elements as the agent of this disequilibrium. Such a model has the advantage of decoupling the REEs from the major elements. It allows the petrologic characteristics and major-element equilibration to be established at high temperatures, while the REE disequilibrium reflects a later low-temperature event. However, there are problems with such a model, particularly as applied to Monument Draw. For example, it would be very difficult to produce an apatite with a positive Eu anomaly and the other apatites and whitlockites with negative Eu anomalies from the same fluid phases. One possibility is that the small interstitial phosphates formed locally via metamorphism while the veins phosphates came in with a fluid phase. Although somewhat poorly constrained, the abundance of phosphates in Monument Draw (~ 0.8 vol%) is somewhat higher than that in ordinary chondrites ($\sim 0.6\%$), suggesting that a phosphate-rich fluid supplied only a small portion of the total phosphate now observed in Monument Draw.

5.4. Chronological History

In this section we address the chronology of acapulcoites and its implications for the thermal history of the parent body. Göpel et al. (1992) reported a precise Pb-Pb isochron age of 4.557 ± 0.002 Ga for U-enriched phosphates in Acapulco. The ^{129}I - ^{129}Xe formation interval between Acapulco phosphates and the Bjurböle chondrite was measured to be only 8 Ma (Nichols et al., 1994). The phosphate age most likely represent metamorphic processes and would define a minimum time of formation for the parent body. Prinzhofer et al. (1992) reported an unusually old Sm-Nd isochron age for Acapulco of 4.60 ± 0.03 , which they interpret to be the time of recrystallization, unaffected by later metamorphism. This age, however, is older than isotopic formation times determined for several other meteorite types. The ^{39}Ar - ^{40}Ar ages of acapulcoites are considerably younger than these other isotopic ages and suggest that the parent body may have undergone a significant period of metamorphism. The questions we now address are why the ^{39}Ar - ^{40}Ar ages for acapulcoites appear younger and what this difference may reveal about the parent body history. To address these questions, we first make comparisons to equivalent data for other meteorites, especially ordinary chondrites.

5.4.1. A comparison of ^{39}Ar - ^{40}Ar ages

Several meteorite types exhibit ^{39}Ar - ^{40}Ar ages substantially younger than the likely formation times of their parent objects. Fourteen unshocked H, L, and LL chondrites give ^{39}Ar - ^{40}Ar ages between 4.44 and 4.52 Ga, with a mean of 4.48 ± 0.03 Ga (Turner et al., 1978). Metamorphic temperatures of type 5–6 chondrites are estimated to have been in the range of ~ 700 – 950°C (Dodd, 1981). Assuming chondrite cooling rates of ~ 10 K/Ma and Ar closure temperatures ($240 \pm 120^\circ\text{C}$) calculated for their samples, Turner et al. (1978) concluded that the younger ^{39}Ar - ^{40}Ar ages of ordinary chondrites represented postmetamorphic cooling times on their parent bodies on the order of 10^8 years. Pellas and Fiéni (1988), considering additional data of unshocked meteorites, found that most dated H, L, and LL chondrites have ^{39}Ar - ^{40}Ar ages in the range of 4.52–4.38 Ga. They suggested that the ^{39}Ar - ^{40}Ar ages of LL chondrites (4.38–.51 Ga) correlates with metamorphic grade, which could be evidence that the age variation was caused by variable cooling times on the parent body. In other studies, Herpfer et al. (1994) noted that the ^{39}Ar - ^{40}Ar and K- ^{40}Ar ages of silicate inclusions from six IAB iron meteorites are 4.447–4.516 Ga, implying lower closure temperatures for the K-Ar system in comparison to the I-Xe system and slower cooling rates at lower temperatures. All of the relatively precise K-Ar ages mentioned above, including the ages for five acapulcoites that we analyzed, as well as other data, were determined in different laboratories and represent several parent bodies. Yet, there is little evidence for accurately determined Ar ages older than ~ 4.53 Ga.

Pb-Pb ages of chondrites also show some variation likely due to metamorphic processes. Hanan and Tilton (1985) reported Pb-Pb ages of 4.480 ± 0.011 and 4.472 ± 0.005 Ga for a L3 and a H3 chondrite, respectively. Göpel et al.

(1994) reported precise Pb-Pb ages of bulk fragments and U-enriched phosphates from six H chondrites (type 4–6), 5 L chondrites (type 5–6), and 3 LL chondrites (type 5–6). Ages of H chondrite phosphates ranged between 4.504 Ga and 4.563 Ga and showed a negative correlation with metamorphic grade. Although interpretation of these Pb ages is model dependent, this correlation presumably reflects phosphate formation during parent body metamorphism and would be consistent with a layered H chondrite parent body. Phosphates from the L chondrites showed a range in age of ~ 4.511 – $.543$ Ga. Göpel et al. (1994) concluded that the ~ 60 Ma time interval observed in the phosphate ages reflected the thermal processing of these equilibrated chondrites on their parent bodies. However, they were unable to decide between early metamorphism followed by slow cooling or partial resetting in later metamorphic events.

The ^{39}Ar - ^{40}Ar ages of most unshocked ordinary chondrites and silicate inclusions in IAB irons show ranges in ages of ~ 80 Ma, similar to the ~ 60 Ma range shown by Pb-Pb ages of H chondrites. However, both the average K-Ar age for a given meteorite group and the maximum K-Ar ages are shifted downward by about 30–50 Ma compared to the corresponding Pb-Pb ages. If we adopt a closure temperature for Pb in chondritic phosphates of $\sim 454^\circ\text{C}$ (Göpel et al., 1994), a closure temperature for Ar in bulk chondrites of $\sim 240^\circ\text{C}$ (Turner et al., 1978), and a cooling rate of 10 K/Ma, we can account for approximately 20 Ma of the difference between these Pb-Pb and K-Ar ages. However, because fission track data for some chondrites suggest that the cooling rate may have been even slower at $< 200^\circ\text{C}$ (Pellas and Storzer, 1979; Pellas, 1981; Pellas and Fiéni, 1988), an even larger age difference may be accommodated. Therefore, one explanation of the observation that ^{39}Ar - ^{40}Ar ages of a variety of meteorite types are younger than 4.55 Ga is that their parent bodies experienced metamorphism that left them above Ar closure temperatures for significant periods of time. Before examining this possible explanation for the acapulcoites, however, we first consider other possible explanations for the younger Ar ages.

5.4.2. Possible biases in ^{39}Ar - ^{40}Ar ages

The ^{39}Ar - ^{40}Ar ages of meteorites depend upon the accuracy of the determined absolute age of a standard sample and of the measured differences in neutron fluence between standard and unknown samples. Because the ^{39}Ar - ^{40}Ar ages quoted above were measured in several laboratories using different neutron fluence monitors, it seems most unlikely that younger Ar ages are due to analytical bias in mass spectrometer measurements or to systematic errors in measuring relative neutron fluence. It also appears unlikely that each of the standard age samples used by these laboratories could have a similar bias in age. The K-Ar age for each age standard was calculated from precise measurements of K and ^{40}Ar made in different laboratories, and for at least two standards these K- ^{40}Ar ages agree with Rb-Sr isochron ages. The analytical uncertainties quoted for these absolute K- ^{40}Ar ages ranged from $< 0.5\%$ up to $\sim 1.9\%$ (Turner et al., 1971; Roddick, 1983). (Hornblende NL-25 used in this study has an absolute age uncertainty of about $\pm 0.5\%$ and is further

described by Bogard et al., 1995). Fortunately, several K-Ar age standards, including those used by all of the laboratories whose meteorite ages are quoted above, have been irradiated together and compared (Alexander and Davis, 1974; Roddick, 1983). The normalized ages of at least six of these ^{39}Ar - ^{40}Ar age standards agree to better than $\pm 0.5\%$, which is a strong argument that their absolute age determinations are accurate to better than $\pm 0.5\%$. We conclude that a systematic uncertainty in the age of the standard samples cannot explain the full amount by which ^{39}Ar - ^{40}Ar ages of most meteorites appear younger than typical formation ages of 4.55–4.56 Ga.

We can also consider effects of uncertainties in the ^{40}K decay constant and the $^{40}\text{K}/\text{K}$ mixing ratio on calculated $^{39}\text{Ar}/^{40}\text{Ar}$ ages. The recommended K decay constants (Steiger and Jaeger, 1977) are those reported by Beckinsale and Gale (1969). The uncertainty in the overall ^{40}K half-life is only 0.18%, but the primary error for Ar dating arises from the uncertainty in the minor decay path that leads to ^{40}Ar . These uncertainties produce an age uncertainty of 13 Ma in a 4.5 Ga old sample (Beckinsale and Gale, 1969). The recommended $^{40}\text{K}/\text{K}$ mixing ratio of 1.167×10^{-4} has an uncertainty of 0.34% (Garner et al., 1975), which produces an age uncertainty in a 4.5 Ga old sample of 6 Ma. Thus, the compounded uncertainty in the absolute age of a 4.5 Ga old sample due to both of these parameters is unlikely to exceed ± 15 Ma.

We can compare these possible biases in K-Ar ages with comparable uncertainties for other isotopic chronometers. The decay constants recommended for U (Steiger and Jaeger, 1977) have a reported error of less than $\pm 0.1\%$ (Jaffey et al., 1971), equivalent to an age uncertainty of $< \pm 5$ Ma for a 4.5 Ga old sample. Ages calculated from U-Pb or Pb-Pb also often have low analytical errors, but in many cases such ages are model dependent. The decay constant in the ^{147}Sm - ^{143}Nd chronometer is apparently known to a precision of about $\pm 0.8\%$ (Lugmair and Marti, 1978), which is equivalent to an uncertainty in absolute age of ± 36 Ma in an 4.5 Ga old sample. The uncertainties in absolute ages of various chronometers caused by errors in decay parameters can, in principle, be reduced by normalizing to the Pb-Pb age of the same sample. For example, from a precise whole-rock Rb-Sr isochron measured for many ordinary chondrites and the ^{87}Rb decay constant of $1.42 \times 10^{-11}/\text{y}$ recommended by Steiger and Jaeger (1977), Minster et al. (1982) calculated a parent body formation age of 4.498 ± 0.015 Ga. In order to force agreement of Rb-Sr data with the U-Pb age of chondrites of 4.555 Ga, these authors suggested the ^{87}Rb decay constant should be $1.402 \times 10^{-11}/\text{y}$, a change of 1.2%. In the case of the LEW 86010 achondrite, one determination of the Pb-Pb age gave 4.55764 ± 0.00052 Ga and two determinations of the Sm-Nd age gave 4.553 ± 0.034 Ga and 4.538 ± 0.033 Ga (Lugmair and Galer, 1992; Nyquist et al., 1993). Other instances exist in the literature where such age comparisons have been made, especially with younger terrestrial samples (e.g., Nunes, 1981).

The discussion above suggests that even precisely determined meteorite ages contain some uncertainty in their absolute values because of possible errors in decay constants, and in the case of ^{39}Ar - ^{40}Ar ages, also in the accuracy of

the age of the standard sample. It seems most unlikely, however, that the total difference between those ^{39}Ar - ^{40}Ar ages of ~ 4.42 – 4.53 Ga and likely formation times of some meteorite parent bodies of ~ 4.55 – 4.56 Ga are due to such biases. The K-Ar chronometer is more readily reset compared to other isotopic chronometers (Shih et al., 1994; Bogard, 1995), and the younger ^{39}Ar - ^{40}Ar ages of meteorites evidently reflect resetting by impact or internal metamorphism after parent body formation. The parent bodies of meteorite groups such as the chondrites and IAB silicates, whose ^{39}Ar - ^{40}Ar ages for unshocked specimens are generally 4.52–4.40 Ga, must have resided at metamorphic temperatures above Ar closure for times ranging from ~ 30 to ~ 150 Ma after parent body formation. It is conceivable that chondritic cooling rates slowed considerably at lower temperatures due to accretion of low diffusivity material to the parent body surface (Warren et al., 1991; Herpfer et al., 1994). Another possible explanation for younger ^{39}Ar - ^{40}Ar ages may be later periods of parent body metamorphism, much milder than the original metamorphism, and arising from internal heating due to the decay of longer-lived nuclides. Reheating meteorite parent bodies to temperatures of 200–300°C after initial cooling might be sufficient to reset K-Ar ages and fission tracks without affecting metallographic cooling rates or other isotopic chronometers having higher closure temperatures.

5.4.3. Thermal history of acapulcoites derived from chronology

The parent object of acapulcoite meteorites may have resembled the parent objects of ordinary chondrites in composition and size and may have formed at about the same time. At least part of the acapulcoite parent reached metamorphic temperatures of $\sim 1000^\circ\text{C}$, higher than that of most chondrites. Cooling rates of ~ 100 K/Ma estimated for Acapulco pyroxenes at 900–1000°C (Zipfel et al., 1995) would require times of only several Ma to cool from metamorphic temperatures to that of Pb closure, which appears consistent with the Pb-Pb age of 4.556 Ga for Acapulco phosphate (Göpel et al., 1992). Metallographic cooling rates estimated here ($\sim 10^3$ – 10^5 K/Ma at $\sim 500^\circ\text{C}$) would indicate even shorter cooling times. Closure of the K-Ar chronometer for at least five acapulcoite meteorites, however, did not occur until 4.51 ± 0.02 Ga ago, which suggests slower cooling at lower temperatures. Fission track data for Acapulco also suggest that the cooling rate slowed considerably to only ~ 2 K/Ma at temperatures $< 300^\circ\text{C}$ (Pellas and Fiéni, 1992). If the average cooling rate for acapulcoite meteorites was 15 K/Ma (somewhat above the minimum average value of 10 K/Ma deduced from Fig. 15), then it would require a time of ~ 50 Ma, mostly at lower temperatures, to cool from $\sim 1000^\circ\text{C}$ to the Ar closure temperature of the high-K/Ca phase ($\sim 250^\circ\text{C}$ for 2 K/Ma). The fact that ^{39}Ar - ^{40}Ar ages of acapulcoites are older than those of most chondrites suggests that the acapulcoite parent body overall cooled faster than typical chondritic parent objects. This may indicate either that the acapulcoite parent was smaller or that it did not experience possible later periods of mild metamorphism. Unlike the case for many ordinary chondrites, the eight aca-

pulcoites dated by K-Ar show no evidence of significant heating by impact events after 4.5 Ga ago.

5.4.4. Ejection from the parent body

Within the uncertainties inherent in the calculation of cosmic ray exposure ages, three of the four acapulcoites for which cosmogenic noble gases have been measured (Acapulco, Monument Draw, and Yamato 74063) have identical ^{21}Ne exposure ages of $\sim 6.5\text{--}8$ Ma. They might, thus, have been produced in a common impact event. An $\sim 20\text{--}25\%$ lower nominal ^{21}Ne exposure age is deduced for the fourth of these meteorites, ALH A77081. It is unclear, however, whether this difference is really significant. The fact that one of the four Acapulco age values discussed above is about 20% higher than the three others reminds us that even shielding corrected ^{21}Ne exposure ages are still uncertain by $\sim 20\%$, at least for very heavily shielded or very lightly shielded samples, as is the case here. In summary, one or possibly two ejection events can explain the available cosmogenic noble gas data in acapulcoites. Noble gases of ALH A81187 and 84190, which have Fa contents distinctly different from the other acapulcoites, have not yet been measured.

5.5. Trapped Noble Gases

The noble gas results reveal one unexpected feature of acapulcoites, namely the relatively high concentrations of trapped ("planetary") noble gases, despite the fact that these meteorites experienced high peak temperatures ($\sim 1000^\circ\text{C}$). Monument Draw (this work), Acapulco (Palme et al., 1981), and ALH A77081 (Schultz et al., 1982) are similar in this respect to type 4 ordinary chondrites and contain nearly an order of magnitude more gas than type 5–6 ordinary chondrites (Loeken et al., 1992). Most remarkably, Takaoka et al. (1993) report trapped gas concentrations for a bulk sample of Y-74063 that are some 50 times above those in Monument Draw. The Y-74063 values are thus even several times higher than those in the most gas-rich carbonaceous chondrites and similar to the highest concentrations in ureilites, which contain the highest amounts of trapped gas (Mazor et al., 1970).

An interesting question thus is whether all acapulcoite precursors initially incorporated similarly large amounts of trapped gases as Yamato 74063 or whether trapped gases were efficiently enriched in this meteorite or its precursor. Unfortunately, elemental ratios are of little use in judging this question. The exceptionally low $^{84}\text{Kr}/^{132}\text{Xe}$ ratio of 0.36 in Monument Draw might suggest noble gas loss by diffusion, but this suggestion is supported neither by the $^{84}\text{Kr}/^{132}\text{Xe}$ ratios of 0.8–0.9 in bulk samples of all other acapulcoites mentioned above nor by the $^{36}\text{Ar}/^{84}\text{Kr}$ ratio of 81 in Monument Draw, the latter values being in the normal range for chondrites. Furthermore, gas-rich Yamato 74063 has a $^{36}\text{Ar}/^{84}\text{Kr}$ ratio 3–4 times lower than other acapulcoites, opposite to what would be expected if the latter had lost gas by diffusion. The low $^{84}\text{Kr}/^{132}\text{Xe}$ ratio in Monument Draw may instead indicate an initially high relative abundance of trapped Xe compared to chondrites or other acapulcoites.

Trapped gases in acapulcoites are stored, at least in part,

in bubbles (Kim and Marti, 1994; Takaoka et al., 1994). In contrast, in carbonaceous chondrites they reside in a carbonaceous carrier dubbed "Q" (Lewis et al., 1975) and a similar HF/HCl-resistant but oxidizable carrier also contains a sizeable fraction of the trapped gas in ordinary chondrites. This suggests that the efficiency of retrapping Q-type gases during metamorphism determines the final gas abundance in acapulcoites. Takaoka et al. (1994) speculate that the extremely high concentrations in Yamato 74063 may have been carried by CO_2 along fractures, whereas Kim and Marti (1994) suggest that partial pressures of noble gases in Yamato 74063 may have been particularly high due to closed system crystallization of minerals or that this meteorite simply contains a particularly large number of voids.

6. CONCLUSIONS

We can now reconstruct a history for the acapulcoites based on the available petrologic, chemical and isotopic constraints presented and discussed above.

- 1) Acapulcoites formed from a precursor chondrite which differs from known chondrites in mineral and oxygen isotopic compositions. This precursor itself probably formed at 4.557 Ga.
- 2) Heating to $\sim 950\text{--}1000^\circ\text{C}$ resulted in melting at the Fe,Ni-FeS cotectic, but silicates did not melt. Silicate textures resulted from extensive solid-state recrystallization. Heating was by noncollisional sources (e.g., ^{26}Al , electromagnetic induction).
- 3) Heating and cooling occurred very early in the history of the solar system, as evidenced by the $^{39}\text{Ar}\text{--}^{40}\text{Ar}$ ages of ~ 4.51 Ga. Acapulcoites experienced a complex thermal history. Available data suggests a three-stage cooling history of moderate cooling at high temperature, fast cooling at intermediate temperature, and slow cooling at low temperature. This might suggest a complex physical history for the acapulcoite parent body, possibly involving collisional breakup and gravitational reassembly.
- 4) One or at most two impact events (~ 7 Ma and possibly ~ 5 Ma ago) are consistent with the cosmic ray exposure ages of all four acapulcoites for which cosmogenic noble gas data exist.

Acknowledgments—We thank the late G.I. Huss, W. Zeitschel, R.S. Clarke, Jr. (Smithsonian), C.B. Moore (ASU), the National Institute of Polar Research, and the Meteorite Working Group for providing acapulcoites for study. Drs. H.Y. McSween Jr. and M.E. Lipschutz provided samples of artificially heated Krymka for examination. We dedicate this paper to the memory of Glenn I. Huss, who first brought Monument Draw to our attention and inspired our work on acapulcoites. We thank G.J. Taylor, E.R.D. Scott, and J.I. Goldstein for helpful discussions. Very helpful reviews by J. Zipfel, C. Göpel, and L. Schultz significantly improved the manuscript. This work was supported in part by NASA grants NAG 9–40, NAGW-3281 (K. Keil), NAGW-3297 (G.J. Wasserburg), RTOP 152–14 (D. Bogard), NSF grant EAR 92–18857 (R. Clayton), and the Swiss National Science Foundation (R. Wieler). This paper is Hawaii Institute of Geophysics and Planetology publication no. 870 and School of Ocean and Earth Science and Technology publication no. 4056 and Caltech Div. Contrib. #5745(871).

Editorial handling: J. N. Grossman

REFERENCES

- Alexander E. C., Jr., and Davis P. (1974) ^{40}Ar – ^{39}Ar ages and trace element contents of Apollo 14 breccias; an interlaboratory cross-calibration of ^{40}Ar – ^{39}Ar standards. *Geochim. Cosmochim. Acta* **38**, 911–928.
- Anders E. and Grevesse N. (1989) Abundances of the elements: Meteoritic and solar. *Geochim. Cosmochim. Acta* **53**, 197–214.
- Beckinsale R. D. and Gale N. H. (1969) A reappraisal of the decay constants and branching ratio of ^{40}K . *Earth Planet. Sci. Lett.* **6**, 289–294.
- Bernius M. T., Hutcheon I. D., and Wasserburg G. J. (1991) Search for evidence of ^{26}Al in meteorites that are planetary differentiates. *Lunar Planet. Sci. XXII*, 93–94 (abstr.).
- Bogard D. D. (1995) Impact ages of meteorites: A synthesis. *Meteoritics* **30**, 244–268.
- Bogard D. D., Garrison D. H., Norman M., Scott E. R. D., and Keil K. (1995) ^{39}Ar – ^{40}Ar age and petrology of Chico: Large scale impact melting on the L chondrite parent body. *Geochim. Cosmochim. Acta* **59**, 1383–1400.
- Brearley A. J. (1989) Nature and origin of matrix in the unique type 3 chondrite, Kakangari. *Geochim. Cosmochim. Acta* **53**, 2395–2411.
- Clayton R. N. and Mayeda T. K. (1963) The use of bromine pentafluoride in the extraction of oxygen from oxides and silicates for isotopic analyses. *Geochim. Cosmochim. Acta* **27**, 43–52.
- Clayton R. N. and Mayeda T. K. (1983) Oxygen isotopes in eucrites, shergottites, nakhlites and chassignites. *Earth Planet. Sci. Lett.* **62**, 1–6.
- Clayton R. N. and Mayeda T. K. (1988) Formation of ureilites by nebular processes. *Geochim. Cosmochim. Acta* **52**, 1313–1318.
- Clayton R. N., Mayeda T. K., Olsen E. J. and Prinz M. (1983) Oxygen isotope relationships in iron meteorites. *Earth Planet. Sci. Lett.* **65**, 229–232.
- Clayton R. N., Mayeda T. K. and Yanai K. (1984) Oxygen isotopic compositions of some Yamato meteorites. *Mem. NIPR Spec. Issue* 35; Proc. 9th Symp. Antarctic Meteor., 267–271.
- Clayton R. N., Mayeda T. K., and Nagahara H. (1992) Oxygen isotope relationships among primitive achondrites. *Lunar Planet. Sci. XXIII*, 231–232 (abstr.).
- Crozaz G. and Zinner E. (1985) Ion probe determinations of the rare earth concentrations of individual meteoritic phosphate grains. *Earth Planet. Sci. Lett.* **73**, 41–52.
- Crozaz G., Pellas P., Bourot-Denise M., de Chazal S. M., Fiéni C., Lundberg L. L., and Zinner E. (1989) Plutonium, uranium and rare earths in the phosphates of ordinary chondrites—the quest for a chronometer. *Earth Planet. Sci. Lett.* **93**, 157–169.
- Curtis D. B. and Schmitt R. A. (1979) The petrogenesis of L-6 chondrites: Insights from the chemistry of minerals. *Geochim. Cosmochim. Acta* **43**, 1091–1103.
- Davis A. M., Prinz M., and Weisberg M. K. (1993) Trace element distributions in primitive achondrites. *Lunar Planet. Sci. XXIV*, 375–376 (abstr.).
- Dodd R. T. (1981) *Meteorites: A Chemical–Petrologic Synthesis*. Cambridge Univ. Press.
- Dodson M. H. (1973) Closure temperatures in cooling geochronological and petrological systems. *Contrib. Mineral. Petrol.* **40**, 259–274.
- El Goresy A., Zinner E., Pellas P., and Caillet C. (1995) Acapulco's graphite menagerie: Diverse carbon and nitrogen isotopic signatures. *Lunar Planet. Sci. XXVI*, 367–368 (abstr.).
- Eugster O. and Weigel A. (1993) Xe–Q in lodranites and a hint for Xe–L. FRO 90011 another lodranite? *Lunar Planet. Sci. XXIV*, 453–454 (abstr.).
- Evans J. C., Reeves J. H., Rancitelli L. A., and Bogard D. D. (1982) Cosmogenic nuclides in recently fallen meteorites: Evidence for galactic cosmic ray variations during the period 1967–1978. *J. Geophys. Res.* **87**, 5577–5591.
- Franchi I. A., Akagi T., and Pillinger C. T. (1992) Laser fluorination of meteorites—Small sample analysis of $\delta^{17}\text{O}$ and $\delta^{18}\text{O}$. *Meteoritics* **27**, 222 (abstr.).
- Garner E. L., Murphy T. J., Gramlich J. W., Paulsen P. J., and Barnes I. L. (1975) Absolute isotopic abundance ratios and the atomic weight of a reference sample of potassium. *J. Res. Natl. Bur. Standards* **79A**, No. 6, 713–725.
- Gooding J. L. and Keil K. (1981) Relative abundances of chondrule primary textural types in ordinary chondrites and their bearing on conditions of chondrule formation. *Meteoritics* **16**, 17–43.
- Göpel Ch., Manhès G. and Allègre C. J. (1992) U–Pb study of the Acapulco meteorite. *Meteoritics* **27**, 226 (abstr.).
- Göpel Ch., Manhès G., and Allègre C. J. (1994) U–Pb systematics of phosphates from equilibrated ordinary chondrites. *Earth Planet. Sci. Lett.* **121**, 153–171.
- Graf T. et al. (1990a) Cosmogenic nuclides and nuclear tracks in the chondrite Knyahinya. *Geochim. Cosmochim. Acta* **54**, 2511–2520.
- Graf T., Baur H., and Signer P. (1990b) A model for the production of cosmogenic nuclides in chondrites. *Geochim. Cosmochim. Acta* **54**, 2521–2534.
- Haack H. and Rasmussen K. L. (1994) Clues to nonlinear thermal histories from metallographic cooling rate determinations. *Meteoritics* **29**, 470–471 (abstr.).
- Haack H., Rasmussen K. L., and Warren P. H. (1990) Effects of regolith/megaregolith insulation on the cooling histories of differentiated asteroids. *J. Geophys. Res.* **95**, 5111–5124.
- Hanan B. B. and Tilton G. R. (1985) Early planetary metamorphism in chondritic meteorites. *Earth Planet. Sci. Lett.* **74**, 209–219.
- Herperfer M. A., Larimer J. W. and Goldstein J. I. (1994) A comparison of metallographic cooling rate methods used in meteorites. *Geochim. Cosmochim. Acta* **58**, 1353–1365.
- Hiroi T. H. and Takeda H. (1991) Reflectance spectroscopy and mineralogy of primitive achondrites-lodranites. *Proc. NIPR Symp. Antarctic Meteor.* **4**, 163–177.
- Huneke J. C., Armstrong J. T., and Wasserburg G. J. (1983) FUN with PANURGE: High mass resolution ion microprobe measurements of Mg in Allende inclusions. *Geochim. Cosmochim. Acta* **47**, 1635–1650.
- Ikramuddin M., Binz C. M., and Lipschutz M. E. (1977) Thermal metamorphism of primitive meteorites—III. Ten trace elements in Krymka L3 chondrite heated at 400–1000°C. *Geochim. Cosmochim. Acta* **41**, 393–401.
- Jaffey A. H., Flynn K. F., Glendenin L. E., Bentley W. C., and Essling A. M. (1971) Precision measurement of half-lives and specific activities of ^{235}U and ^{238}U . *Phys. Rev.* **4C**, 1889–1906.
- Jarosewich E. (1990) Chemical analyses of meteorites: A compilation of stony and iron meteorite analyses. *Meteoritics* **25**, 323–338.
- Jolliff B. L., Haskin L. A., Solson R. O., and Wadhwa M. (1993) Partitioning in REE-saturating minerals: Theory, experiment, and modelling of whitlockite, apatite and evolution of lunar residual magmas. *Geochim. Cosmochim. Acta* **57**, 4069–4094.
- Kallemeyn G. W. and Wasson J. T. (1985) The compositional classification of chondrites: IV. Ungrouped chondritic meteorites and clasts. *Geochim. Cosmochim. Acta* **49**, 261–270.
- Kaneoka I., Takaoka N., and Yanai K. (1992) ^{40}Ar – ^{39}Ar analyses of Antarctic meteorites Y-74063 and ALH-78230: Consortium study of unique meteorites from Antarctica. *Proc. NIPR Symp. Antarctic Meteor.* **5**, 224–232.
- Keil K., Kirchner E., Gomes C. B., and Nelen J. (1977) Studies of Brazilian meteorites V. Evidence for shock metamorphism in the Paranaíba, Mato Grosso, chondrite. *Revista Brasileira de Geociências* **7**, 256–268.
- Keil K., Bell J. F., and Britt D. T. (1992) Reflection spectra of shocked ordinary chondrites and their relationship to asteroids. *Icarus* **98**, 43–53.
- Keil K., Haack H., and Scott E. R. D. (1994) Catastrophic fragmentation of asteroids: Evidence from meteorites. *Planet. Space Sci.* **42**, 1109–1122.
- Kennedy A. K. and Hutcheon I. D. (1992) Chemical and isotopic constraints on the formation of SA-1, a basaltic Allende plagioclase-olivine inclusion. *Meteoritics* **27**, 539–559.
- Kennedy A. K., Lofgren G. E., and Wasserburg G. J. (1993) An experimental study of trace element partitioning between olivine, orthopyroxene and melt in chondrules: Equilibrium values and kinetic effects. *Earth Planet. Sci. Lett.* **115**, 177–195.
- Kim Y. and Marti K. (1994) Isotopic evolution of nitrogen and

- trapped xenon in the Acapulco parent body. *Meteoritics* **29**, 482–483 (abstr.).
- Kretz R. (1982) Transfer and exchange equilibria in a portion of the pyroxene quadrilateral as deduced from natural and experimental data. *Geochim. Cosmochim. Acta* **46**, 411–421.
- Kubaschewski O. (1982) *Iron–Binary Phase Diagram*. Springer.
- Kullerød G. (1963) The Fe–Ni–S system. *Ann. Rep. Geophys. Lab* **67**, 4055–4061.
- Lavielle B. and Marti K. (1992) Trapped Xe in ordinary chondrites. *J. Geophys. Res.* **97**, E12, 20875–20881.
- Lewis R. S., Srinivasan B., and Anders E. (1975) Host phase of a strange xenon component in Allende. *Science* **190**, 1251–1262.
- Loeken Th., Scherer P., Weber H. W., and Schultz L. (1992) Noble gases in eighteen stone meteorites. *Chem. Erde* **52**, 249–259.
- Lugmair G. W. and Galer S. J. G. (1992) Age and isotopic relationships among the angrites Lewis Cliff 86010 and Angra dos Reis. *Geochim. Cosmochim. Acta* **56**, 1673–1694.
- Lugmair G. W. and Marti K. (1978) Lunar initial $^{143}\text{Nd}/^{144}\text{Nd}$: Differential evolution of the lunar crust and mantle. *Earth Planet. Sci. Lett.* **39**, 349–357.
- Marti K., Kim Y., Yang C. W., Goldstein J. I., and Lavielle B. (1994) Acapulco: Constraining the cooling history of a parent body. *Meteoritics* **29**, 496 (abstr.).
- Mason B. (1995) Thin section description of QUE 93148. *Antarctic Meteor. Newslett.* **18**, No. 1, 15.
- Mazor E., Heymann D., and Anders E. (1970) Noble gases in carbonaceous chondrites. *Geochim. Cosmochim. Acta* **34**, 781–824.
- McCoy T. J., Steele I. M., Keil K., Leonard B. F., and Endreß M. (1994) Chladniite, $\text{Na}_2\text{CaMg}_7(\text{PO}_4)_6$: A new mineral from the Carlton (IIICD) iron meteorite. *Amer. Mineral.* **79**, 375–380.
- McCoy T. J., Keil K., Clayton R. N., Mayeda T. K., Bogard D. D., Garrison D. H., and Wieler R. (1996a) A petrologic and isotopic study of lodranites: Evidence for early formation as partial melt residues from heterogeneous precursors. *Geochim. Cosmochim. Acta* (submitted).
- McCoy T. J., Keil K., Muenow D. W., and Wilson L. (1996b) Partial melting and explosive volcanism on the acapulcoite–lodranite parent body. *Geochim. Cosmochim. Acta* (submitted).
- McSween H. Y., Jr., Taylor L. A. and Lipschutz M. E. (1978) Metamorphic effects in experimentally heated (L3) chondrite. *Proc. 9th Lunar Planet. Sci. Conf.*, 1437–1447.
- McSween H. Y., Jr., Bennett M. E., III, and Jarosewich E. (1991) The mineralogy of ordinary chondrites and implications for asteroid spectroscopy. *Icarus* **90**, 107–116.
- Melosh H. J. (1989) *Impact Cratering: A Geologic Process*. Oxford Univ. Press.
- Minster J. F., Birck J. L., and Allègre C. J. (1982) Absolute age of formation of chondrites studied by the ^{87}Rb – ^{87}Sr method. *Nature* **300**, 414–419.
- Mittlefehldt D. W., Lindstrom M. M., Bogard D. D., Garrison D. H., and Field S. W. (1996) Acapulco- and Lodran-like achondrites: Petrology, geochemistry, chronology, and origin. *Geochim. Cosmochim. Acta* **60**, 867–882.
- Murrell M. T., Brandriss M., Woolum D. S., and Burnett D. S. (1984) Pu–REE–Y partitioning between apatite and whitlockite. *Lunar Planet. Sci.* **XV**, 579–580 (abstr.).
- Nichols R. H., Jr., Hohenberg C. M., Kehm K., Kim Y., and Marti K. (1994) I–Xe studies of the Acapulco meteorite: Absolute I–Xe ages of individual phosphate grains and the Bjurböle standard. *Geochim. Cosmochim. Acta* **58**, 2553–2561.
- Nishiizumi K., Regnier S., and Marti K. (1980) Cosmic ray exposure ages of chondrites, pre-irradiation and constancy of cosmic ray flux in the past. *Earth Planet. Sci. Lett.* **50**, 156–170.
- Nunes P. D. (1981) The age of the Stillwater Complex: A comparison of U–Pb zircon and Sm–Nd isochron systematics. *Geochim. Cosmochim. Acta* **45**, 1961–1963.
- Nyquist L. E., Wiesmann H., Bansal B. M., and Shih C. Y. (1993) Isotopic studies of angrite LEW 86010 and the early history of its parent body. *Meteoritics* **28**, 414–415 (abstr.).
- Palme H. et al. (1981) The Acapulco meteorite: Chemistry, mineralogy and irradiation effects. *Geochim. Cosmochim. Acta* **45**, 727–752.
- Pellas P. (1981) Early thermal histories of L chondrites. *Lunar Planet. Sci.* **XII**, 825–826 (abstr.).
- Pellas P. and Fiéni C. (1988) Thermal history of ordinary chondrite parent asteroids. *Lunar Planet. Sci.* **XIX**, 915–916 (abstr.).
- Pellas P. and Fiéni C. (1992) ^{244}Pu content of phosphates and cooling history of Acapulco meteorite. *Lunar Planet. Sci.* **XXIII**, 1051–1052 (abstr.).
- Pellas P. and Storzer D. (1979) Differences in the early cooling histories of the chondritic asteroids. *Meteoritics* **14**, 513–515 (abstr.).
- Prinz M., Nehru C. E., Delaney J. S., and Weisberg M. (1983) Silicates in IAB and IIICD irons, winonaites, lodranites and Brachina: A primitive and modified primitive group. *Lunar Planet. Sci.* **XIV**, 616–617 (abstr.).
- Prinzhofer A., Papanastassiou D. A., and Wasserburg G. J. (1992) Samarium–neodymium evolution of meteorites. *Geochim. Cosmochim. Acta* **56**, 797–815.
- Richardson S. M. and McSween H. Y., Jr. (1989) *Geochemistry: Pathways and Processes*. Prentice Hall.
- Roddick J. C. (1983) High precision intercalibration of ^{40}Ar – ^{39}Ar standards. *Geochim. Cosmochim. Acta* **47**, 887–898.
- Schelhaas N., Ott U., and Begemann F. (1990) Trapped noble gases in unequilibrated ordinary chondrites. *Geochim. Cosmochim. Acta* **54**, 2869–2882.
- Schultz L., Palme H., Spettel B., Weber H. W., Wänke H., Christophe Michel–Levy M., and Lorin J. C. (1982) Allan Hills A77081–An unusual stony meteorite. *Earth Planet. Sci. Lett.* **61**, 23–31.
- Score R. and Lindstrom M. M. (1990) Guide to the U.S. Collection of Antarctic Meteorites 1976–1988. *Antarctic Meteorite Newsletter* **13**, No. 1.
- Shih C.-Y., Nyquist L. E., Bogard D. D., and Wiesmann H. (1994) K–Ca and Rb–Sr dating of two lunar granites: Relative chronometer resetting. *Geochim. Cosmochim. Acta* **58**, 3101–3116.
- Steiger R. H. and Jaeger E. (1977) Subcommittee on geochronology: Convention on the use of decay constants in geo- and cosmochemistry. *Earth Planet. Sci. Lett.* **36**, 359–362.
- Stöffler D., Keil K., and Scott E. R. D. (1991) Shock metamorphism of ordinary chondrites. *Geochim. Cosmochim. Acta* **55**, 3845–3867.
- Takahashi E. (1983) Melting of a Yamato L3 chondrite (Y–74191) up to 30 kbar. *Mem. NIPR Spec. Issue 30; Proc. 8th Symp. Antarctic Meteor.*, 168–180.
- Takaoka N. and Yoshida Y. (1991) Noble gas composition in unique meteorite Yamato-74063. *Proc. NIPR Symp. Antarctic Meteor.* **4**, 178–186.
- Takaoka N., Nagao K., and Miura Y. (1993) Noble gases in the unique meteorites Yamato-74063 and -74357. *Proc. NIPR Symp. Antarctic Meteor.* **6**, 120–134.
- Takaoka N., Motomura Y., Ozaki K., and Nagao K. (1994) Where are noble gases trapped in Yamato–74063 (Unique)? *Proc. NIPR Symp. Antarctic Meteor.* **7**, 186–196.
- Takeda H. and Miyamoto M. (1994) Orthopyroxene with dusty core and clear rims in Acapulco and its related formation processes to Lodranites. *Lunar Planet. Sci.* **XXV**, 1371–1372 (abstr.).
- Takeda H., Mori H., Yanai K. and Shiraiishi K. (1980) Mineralogical examination of Allan Hills achondrites and their bearing on the parent bodies. *Mem. NIPR Spec. Issue 17; Proc. 5th Symp. Antarctic Meteor.*, 119–144.
- Takeda H., Saiki K., Otsuki M., and Hiroi T. (1993) A new Antarctic meteorite with chromite, orthopyroxene and metal with reference to a formation model of S asteroids. *Lunar Planet. Sci.* **XXIV**, 1395–1396 (abstr.).
- Takeda H., Mori H., Hiroi T., and Saito J. (1994) Mineralogy of new Antarctic achondrites with affinity to Lodran and a model for their evolution in an asteroid. *Meteoritics* **29**, 830–842.
- Taylor G. J., Keil K., McCoy T., Haack H., and Scott E. R. D. (1993) Asteroid differentiation: Pyroclastic volcanism to magma oceans. *Meteoritics* **28**, 34–52.
- Torigoye N., Yamamoto K., Misawa K., and Nakamura N. (1993) Compositions of REE, K, Rb, Sr, Ba, Mg, Ca, Fe and Sr isotopes in Antarctic “unique” meteorites. *Proc. NIPR Symp. Antarctic Meteor.* **6**, 100–119.

- Turner G., Huneke J. C., Podosek F. A. and Wasserburg G. J. (1971) ^{40}Ar - ^{39}Ar ages and cosmic ray exposure ages of Apollo 14 samples. *Earth Planet. Sci. Lett.* **12**, 19–35.
- Turner G., Enright M. C., and Cadogan P. H. (1978) The early history of chondrite parent bodies inferred from ^{40}Ar - ^{39}Ar ages. *Proc. 9th Lunar Planet. Sci. Conf.*, 989–1025.
- Van Schmus W. R. and Ribbe P. H. (1968) The composition and structural state of feldspar from chondritic meteorites. *Geochim. Cosmochim. Acta* **32**, 1327–1342.
- Warren P. H., Haack H., and Rasmussen K. L. (1991) Megaregolith insulation and the duration of cooling to isotopic closure within differentiated asteroids and the moon. *J. Geophys. Res.* **96**, B4, 5909–5923.
- Wieler R., Anders E., Baur H., Lewis R. S., and Signer P. (1991) Noble gases in “phase Q”: Closed-system etching of an Allende residue. *Geochim. Cosmochim. Acta* **55**, 1709–1722.
- Willis J. and Goldstein J. I. (1981) A revision of the metallographic cooling rate curves for chondrites. *Proc. 12th Lunar Planet. Sci. Conf.*, 1135–1143.
- Wood J. A. (1967) Chondrites: Their metallic minerals, thermal histories and parent planets. *Icarus* **6**, 1–49.
- Yanai K. (1984) Locality map series of Antarctic meteorites. Sheet 1. Allan Hills. NIPR.
- Yanai K. and Kojima H. (1987) *Photographic catalog of the Antarctic meteorites*. NIPR.
- Yanai K. and Kojima H. (1991) Yamato-74063: Chondritic meteorite classified between E and H chondrite groups. *Proc. NIPR Symp. Antarctic Meteor.* **4**, 118–130.
- Yugami K., Miyamoto M., Takeda H., and Hiroi T. (1993) Mineralogy of ALH81187: A partly reduced acapulcoite. *Papers Presented to the 18th Symp. Antarct. Met.*, 34–37 (abstr.). NIPR.
- Zinner E. and Crozaz G. (1986) Ion probe determinations of the abundances of all the rare earth elements in single mineral grains. In *Secondary Ion Mass Spectrometry (SIMS V)* (ed. A. Benninghoven et al.), pp. 444–446. Springer-Verlag.
- Zipfel J. and Palme H. (1993) Chemical compositions of new acapulcoites and lodranites. *Lunar Planet. Sci.* XXIV, 1579–1580 (abstr.).
- Zipfel J., Palme H., Kennedy A. K., and Hutcheon I. D. (1995) Chemical composition and origin of the Acapulco meteorite. *Geochim. Cosmochim. Acta* **59**, 3607–3627.